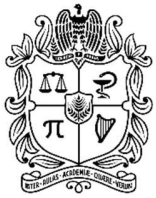

UNIVERSIDAD
NACIONAL
DE COLOMBIA

# Modelo computacional y experimental del comportamiento mecánico y biológico de fibroblastos aislados del ligamento colateral de la rodilla expuestos a estímulos biofísicos del ultrasonido

**Rosy Paola Cárdenas Sandoval**

Universidad Nacional de Colombia
Facultad de Ingeniería, Departamento de Ingeniería Mecánica y Mecatrónica
Bogotá, Colombia
2019

# Modelo computacional y experimental del comportamiento mecánico y biológico de fibroblastos aislados del ligamento colateral de la rodilla expuestos a estímulos biofísicos del ultrasonido

**Rosy Paola Cárdenas Sandoval**

Tesis presentada como requisito parcial para optar al título de:
**Doctor(a) en Ingeniería**

Director (a):
Ph.D., Diego Alexander Garzón Alvarado
Codirector (a):
Ph.D., Alba Graciela Ávila Bernal

Línea de Investigación:
Estímulos biofísicos en Ingeniería de Tejidos / Mecánica celular
Grupo de Investigación:
Grupo Mecanobiología de órganos y tejidos

Universidad Nacional de Colombia
Facultad de Ingeniería, Departamento de Ingeniería Mecánica y Mecatrónica
Bogotá, Colombia
2019

# Computational modeling and in vitro testing of the mechanical and biological properties of collateral knee ligament fibroblasts treated with therapeutic ultrasound

by

**Rosy Paola Cárdenas Sandoval**

A Thesis submitted for the degree of

**Doctor in Engineering**

Universidad Nacional de Colombia

Faculty of Engineering, Department of Mechanical and Mechatronics Engineering

Bogotá, Colombia

2019

*Dedicatoria*

*A mi familia*

*Por acompañarme en este camino, por ser mi soporte en los momentos de agobio, por estimularme y creer en mis habilidades para alcanzar esta meta.*

## Agradecimientos

A mis mentoras: PhD. Alba Avila Bernal, Profesora asociada al departamento de Ingeniería Eléctrica y Electrónica de la Universidad de los Andes; PhD. Angélica María Ramírez Martínez, Profesora asociada al Departamento de Ingeniería Mecánica de la Universidad Central, PhD Myriam Lucía Navarrete Jiménez, Profesora asociada, Departamento de Microbiología Universidad Nacional, por sus enseñanzas y ejemplo de vida como mujeres científicas;

A mi director de tesis, PhD. Diego Alexander Garzón Alvarado, Profesor titular del Departamento de Ingeniería Mecánica y Mecatrónica de la Universidad Nacional de Colombia por darme la oportunidad de resolver un problema de investigación en una de las profesiones más humanas y aquella dedicada al estudio del movimiento corporal humano, la fisioterapia.

A mi compañero PhD Homero Fernando Pastrana Rendón, Investigador Universidad de los Andes, por todas las luchas y logros en la dura tarea de la investigación in vitro.

A mis tutores: PhD Alejandro Oyono Ondo Méndez, Profesor asociado del Departamento de Ciencias Biomédicas, Escuela de Medicina y Ciencias de la Salud de la Universidad del Rosario, PhD Dionisio Humberto Malagón Romero Dionisio Malagón, Profesor Facultad de Ingeniería Mecánica de la Universidad Santo Tomás, por su orientación académica en el instante preciso de mi formación académica.

En general a todas aquellas personas que vivieron de cerca la realización de esta tesis doctoral, mis sinceros agradecimientos por el apoyo, fraternidad y aliento en los momentos difíciles.

## Resumen

El objetivo de esta tesis fue modelar computacional y experimentalmente el comportamiento mecánico y biológico de fibroblastos del ligamento colateral de la rodilla expuestos a estímulos biofísicos del ultrasonido. Tratamiento con ultrasonido pulsátil a una frecuencia de 1.0 MHz con dos intensidades diferentes 1.0 W/cm$^2$ (Grupo A) y 2.0 W/cm$^2$ (Grupo B) fue aplicado cada 24 horas por cinco días a cultivos monocapa de fibroblastos de ligamento. Un grupo control no recibió tratamiento (Grupo C). La autora midió el módulo de elasticidad celular a través del ensayo con Microscopio de Fuerza Atómica (AFM), armónicos utilizando el Método de los Elementos Finitos (FEM), viabilidad a través de la técnica de citometría de flujo, proliferación por medio de un ensayo colorimétrico (MTS), síntesis de colágeno tipo I y III, y fibronectina mediante el Ensayo de Inmunoabsorbancia Ligado a Enzimas (ELISA), y migración celular a través del ensayo de lesión por raspado. Los resultados mostraron una disminución en el módulo de elasticidad (22% y 32%, $p<0.05$), en los armónicos (20% y 20%) y en la viabilidad celular (1% y 10%) para la baja y alta intensidad, respectivamente. La proliferación celular fue aumentada 10% (Grupo A) y disminuida 13% (Grupo B) ($p<0.05$). El colágeno tipo I fue aumentado 100% para la alta intensidad, y no hubo expresión de colágeno tipo III para la baja intensidad ni para el grupo control. La producción de fibronectina fue aumentada 79% (Grupo A) y 61% (Grupo B). Se comprobó que la disminución del módulo de elasticidad se produjo por una reorganización del citoesqueleto de la célula para 1) proliferar y migrar (aumento del 4%) a la zona de lesión ante baja intensidad de tratamiento y para 2) producir matriz extracelular en la zona de lesión y por tanto disminuir la migración celular (11%) para el tratamiento con alta intensidad ($p<0.05$). Estos hallazgos mostraron que baja dosis de ultrasonido puede estimular la etapa temprana o regenerativa de reparación y alta dosis de tratamiento estimula la etapa tardía o de remodelado. Este trabajo sugiere que el ultrasonido pulsátil estimula a las células para mejorar el proceso de reparación de los ligamentos.

**Palabras clave: fibroblastos, ligamento, ultrasonido pulsátil, módulo de elasticidad, armónicos, viabilidad, proliferación, proteínas de matriz extracelular, migración.**

## Abstract

The aim of this thesis was develop a computational modeling and in vitro testing of the mechanical and biological properties of collateral knee ligament fibroblasts treated with therapeutic ultrasound. Pulsed ultrasound at 1.0 MHz with two different intensities 1.0 W/cm$^2$ (Group A) and 2.0 W/cm$^2$ (Group B) was applied every 24 hours for five days to ligament fibroblasts monolayer cultured. Group C was untreated control group. The author measured cell elastic modulus using an Atomic Force Microscopy (AFM) testing, harmonics with Finite Element Method (FEM), viability by flow cytometry analysis, proliferation via colorimetric assay (MTS), synthesis of type I, type III collagen and fibronectin using the Enzyme Linked Immunosorbent Assay (ELISA) assay, and cell migration through wound scratch assay. The results showed a decreased cell elastic modulus (22% and 31%, $p<0.05$), harmonics (20% and 20%), and viability (1% and 10%) due low and high intensity, respectively. Cell proliferation was raised 10% (Group A) and diminished 13% (Group B) ($p<0.05$). Type I collagen was increased 100% for high intensity, and no detectable type III collagen for low intensity and control group was observed. Fibronectin production was increased 79% (Group A) and 61% (Group B). It was showed that elastic modulus was decreased due cytoskeleton rearrangement to allow cell 1) migration (increased 4%) for low intensity and 2) production of extracellular matrix for high intensity stimulation, thus migration decreased 11% ($p<0.05$). These findings showed that low dose of ultrasound may improve early or regenerative stage of healing and high dose may stimulate late or remodeling phase. This work argued that pulsed therapeutic ultrasound might be used to stimulate cells to improve the ligament healing process.

**Keywords: ligament fibroblasts, pulsed ultrasound, elastic modulus, harmonics, viability, proliferation, extracellular matrix proteins, migration.**

## Table of contents

**Page.**

## List of Figures

**Page**

## List of tables

**Page**

# Introduction

Ligament injuries, also called sprains, are a common musculoskeletal disorder that affect the movement of the human body (Dale et al. 2017; Read et al. 2016; Rincón Cardozo et al. 2015). When a ligament is injured, the joint loses its stability and proprioception (Pedraza Mejías and Martínez Cañadas 2008) increasing the risk of falling-off, and in a long term, may even increase the risk of osteoarthritis (Wheaton and Jensen 2011).

Ligaments are connective tissue made up by cells (fibroblasts), water (two-thirds), and solid components (one-third) conformed by extracellular matrix (mainly collagen, proteoglycans, elastin, and glycoproteins as fibronectin, actin, integrins and laminin) (Wheaton and Jensen 2011); specifically, fibroblasts maintain and repair the extracellular matrix (Pedraza Mejías and Martínez Cañadas 2008).

When a ligament injury occurs, the healing process begins. The simplified phases of the healing process are hemorrhaging and inflammation (the first 72 h following an injury), proliferation (48 h – 6 weeks after the injury), and remodeling (weeks and months). The objective of each one of the healing stages is to remove the damaged tissue, produce a scar tissue, and remodel the matrix similar to the previous uninjured tissue (Wheaton and Jensen 2011).

To stimulate the stages of the ligament healing process, physiotherapists use several physical agents: ice and compression are used to decrease the hemorrhage and swelling (Cárdenas Sandoval et al. 2012; van den Bekerom et al. 2013) and, heat and mechanical stimuli, as elongation and therapeutic ultrasound, are applied to stimulate fibroblasts proliferation and remodeling tissue (Cárdenas Sandoval et al. 2012; Lu et al. 2006). Nevertheless, contradictory effects of ultrasound on ligament healing have been evidenced according to scientific research literature.

Van Den Bekerom et al., found that ultrasound produced 20% of pain relief and decreased 25% of swelling (Van Den Bekerom et al. 2011). Morishita et al., reported that active and passive range of motion was significantly higher by ultrasound (Morishita et al. 2014).

Charly Daniel has shown that combining ultrasound with other therapeutic modalities were found to be more beneficial in the ligament injuries treatment (Charly Daniel 2017). Conversely, researchers reported no pain reduction nor swelling, improvement of the joint functioning and range of motion in humans (Díaz and Fernández 2002; Van Den Bekerom et al. 2011; Warden et al. 2008).

Since studies in humans are limited to explain the effect of ultrasound on the specific properties and function of the ligaments, animal experimentation an in vitro testing are used. Animal studies showed that ultrasound increased the tissue strength (elastic modulus), ultimate load, energy absorption, collagen fibril diameter, relative proportion, and organization (Fu et al. 2008; Leung et al. 2006; Sparrow et al. 2005; Warden et al. 2006a)

In vitro studies demonstrated that ultrasound increased cell proliferation (Cárdenas-Sandoval et al. 2014; Harle et al. 2001a), synthesis of proteins of the extracellular matrix (collagen and glycoproteins) on human dermal, murine embryo ant tendon fibroblasts (Bohari et al. 2015; Choi et al. 2011; Farcic et al. 2013; Freitas et al. 2010; Roper et al. 2012; Shyh-Hau et al. 2003; Tsai et al. 2006; Ying et al. 2012). Ultrasound also activated the pathway and cell migration into the wound (Roper et al. 2015; Tsai et al. 2008).

Moreover, the stimuli induced unstable cavitation (Dyson 1982; Yadollahpour 2014) and a resonance effect as well (Lennart 2002). When unstable cavitation (microbubbles expand and then collapse close to cells (Izadifar et al. 2017; Lennart 2002) and/or a resonance effect (once frequency of ultrasound coincides with the natural frequencies of vibration of cells) is produced, it can be deleterious to cells (Izadifar et al. 2017; Lennart 2002).

To improve the understanding of the effect of ultrasound on tissues computational modeling has also been attempted. Shiran et al., simulated the thermal distribution profile in prostate tumor by ultrasound, finding a rise of temperature on tumors due to several ultrasound intensities (Shiran et al. 2013). Similar computational results showed how high-intensity focused ultrasound can ablate tumors by increasing temperature (Özdemir 2011; Solovchuk et al. 2014) and modulate tissue function as in Parkinson disease (Tarnaud et al. 2018; Mizera & Gambin 2011).

Nevertheless, there are limited studies focused on the effect of therapeutic ultrasound specifically on the biological and mechanical properties of ligament fibroblasts. Harle et al., reported that low intensity ultrasound increased 20% proliferation on periodontal ligament

fibroblasts (Harle et al. 2001a), but no information is reported about mechanical effects of ultrasound on ligament fibroblasts as resistance to deformation or harmonics.

In vitro testing and computational modeling can help to examine the impact of therapeutic ultrasound on fibroblast function during the ligament healing process. The task of the cells can be studied by measuring their ability to resist stresses by external stimuli (elastic modulus), live, proliferate, migrate, and produce extracellular matrix.

We were aimed to evaluate the effect of therapeutic ultrasound on the mechanical and biological properties of ligament fibroblasts. Two doses of pulsed ultrasound 1.0 W/cm$^2$ and 2.0 W/cm$^2$ at a frequency of 1.0 MHz, used in physiotherapy to treat the ligament injuries, with 50% of duty cycle and effective radiation area (ERA) of 5 cm$^2$ were applied on monolayer culture of ligament fibroblasts.

As cells rearrange their cytoskeleton to respond to external stimuli (cell elastic modulus), we hypothesized that therapeutic ultrasound produced variations on the cell elastic modulus to facilitate cell migration into a wounded area. Hence, we assessed cell elastic modulus through Atomic Force Microscopy (AFM) testing and cell migration by scratch assay.

Moreover, we inquired if ultrasound produced a resonance effect that could induce alterations or death in cells. Consequently, to predict a resonance effect we calculated the harmonics of the cell cytoskeleton by computational modelling using the eigenvalue extraction method Lanczos (ABAQUS/CAE 6.12.3 software), and to detect cells that were damaged or dying we assessed fibroblast viability through fluorochrome staining (annexin and propidium iodide by flow cytometry assay).

As cells can modify their cycle or metabolic activity due to stimulation as well, we postulated that therapeutic ultrasound encourages: 1) Cell proliferation to increase the cell number in the injured area, 2) Collagen synthesis to increase the amount of fibers that will provide the resistance to the new tissue, 3) Fibronectin production to facilitate cell migration as well, and 4) cell migration to rise-up the cell displacement into a wounded area.

To proof those hypothesis we measured cell proliferation by cell enzyme activity through colorimetric assay (MTS); proteins synthesis (type I, type III collagen and fibronectin) via

Enzyme Linked Immunosorbent Assay (ELISA); and cell migration with scratch assay using a Cytation 3 Cell Imager Multi-Mode Reader (Biotek), and the software Gen 5.2.0 and ImageJ version 1.50i 3.

To demonstrate that pulsed ultrasound produced non thermal effects we used a computational modeling. We calculated the temperature and acoustic pressure produced by ultrasound at 1.0 MHz on the monolayer cell culture of ligament fibroblasts using the software COMSOL Multyphysics 5.2. Thus, we showed that pulsed therapeutic ultrasound effects on ligament cells were produced by mechanical stimulation.

The results showed a decreased cell elastic modulus (22% and 31%), harmonics (20% and 20%) with non-resonance effect, and viability (1% and 10%) due ultrasound doses (1.0 W/cm$^2$ and 2.0 W/cm$^2$). Type I collagen was increased 100% for high intensity, and no synthesis was detected for low intensity and control group. Fibronectin was increased 79% and 61% for low and high intensity, respectively. Five days after treatment, protein synthesis was also measured. Type I and type III collagen was increased 45% and 71% for high intensity, and increased 30% and 33% for low intensity. Fibronectin was decreased 33% for treatment at 1.0 W/cm$^2$ and increased 44% for treatment at 2.0 W/cm$^2$ ($p<0.05$).

Proliferation and migration were increased 10% and 4% for ultrasound treatment at 1.0 W/cm$^2$, and decreased 13% and 11% at 2.0 W/cm$^2$, respectively. We conclude that cells produced lowest collagen concentration when showed higher fibronectin synthesis, proliferation and migration at 1.0 W/cm$^2$, and vice versa results were detected at 2.0 W/cm$^2$ dose.

The several key contributions of this work are: 1) Propose specific doses of therapeutic ultrasound that can stimulate fibroblasts to improve proliferation and remodeling phases of the ligament healing process, and 2) Complement the state-of-the-art about the influence of pulsed therapeutic ultrasound on the mechanical and biological properties of ligament fibroblasts.

# 1. Effect of the ultrasound stimuli on fibroblast elasticity and harmonic vibration

## 1.1 Introduction

Knee ligament injuries are one of the most common musculoskeletal disorders incurred by young people and adults (Dale et al. 2017; Read et al. 2016). The healing process is initiated by fibroblasts, which are the cells that proliferate and migrate to the injury zone to produce and remodel the new extracellular matrix of the ligament (William E. Prentice 2013).

The cytoskeleton is the structure responsible for regulating the mechanical behavior of the cell; it maintains the cell integrity/structure, responds to external mechanical cues, exerts forces, and produces motion (Samandari, Abrinia, Mokhtari-Dizaji, & Tamayol, 2017; Allsop & Peckham, 2011; Nick, 2011). It comprises a complex interconnected network of actin filaments, intermediate filaments, and microtubules (Nick 2011). Therefore, the cytoskeleton is a fundamental structure in the cell and has an important role in the ligament healing, specially, in the knee ligament.

Since the 1950s, ligament injury has commonly been treated using therapeutic ultrasound with a frequency between 1 and 3 MHz (Miller et al., 2012; O'Brien Jr., 2007), although, nowaday, little is known about its effect on fibroblast structure (Louw, Budhiraja, Viljoen, & Subramanian, 2013; De Deyne & Kirsch-Volders, 1995). According to Samandari et al. (2017), "ultrasonic waves could disrupt/fluidize actin filaments in the cytoskeleton and thus could affect cellular organization" (Samandari et al. 2017).

Consequently, changes in the cytoskeleton structure may affect its mechanical properties, such as the elastic modulus (Wagner et al. 2009), which is defined by Franze (2013) as "the property of a material to deform in response to a force and to return to its original state

once the force is removed" (Franze, 2013; Nijenhuis, Zhao, Carisey, Ballestrem, & Derby, 2014). Thus, the cytoskeleton is implied into the healing and in the mechanical properties before and afterward the damaged ligament and the mechanical behavior of the tissue.

The elastic modulus of the cytoskeleton and the cell is related to a wide variety of biological cellular responses such as communication with the environment, cell death, differentiation, aging, pathophysiology of the disease, and cellular motility (Nijenhuis et al., 2014; Nikolaev, Müller, Williams, & Liu, 2014; Schulze et al., 2017), and it can also influence the harmonic vibration (natural frequencies of vibration) of the cells (Geltmeier et al. 2015). The harmonic vibration of the structure is the rate at which it oscillates at a point of balance without being affected by an external force (Shekofteh et al. 2016).

This mechanical property is important when the periodic force producing by an external stimulus such as the ultrasound coincides with the harmonic vibration of the cell, if this occurs the oscillation may compromise the integrity of the structure owing to the resonance effect (Lepeschkin & Goldman, 1952; Geltmeier et al., 2015; Iranmanesh et al., 2016; Mariantonietta et al., 2015). Trendowski et al. (2015) found that, likely as a result of cytoskeleton involvement, ultrasound frequencies between 20 kHz and 60 kHz can induce lysis and cell death, which occurs in cavitation ultrasound (Trendowski, Christen, Zoino, Acquafondata, & Fondy, 2015; Miller et al., 2012; Wu & Nyborg, 2008; Bandyopadhyay et al., 2016).

However, when there is no resonance effect, the mechanical energy produced by ultrasound is absorbed and modulated by the cell's proteins (Lennart 2002) through a process of assembly of the actin proteins and microtubules (Louw et al., 2013; Noriega, Hasanova, & Subramanian, 2013), which may stimulate other healing steps such as cell migration (Tsai et al. 2008).

So far, studies dealing with the influence of different low-pulsed energy doses of ultrasound on elastic modulus, harmonic vibration and cell death of ligament fibroblasts are rare (Jiang et al. 2015).

The approach described in this research complements clinical rehabilitation to find a standard prescription of ultrasonic that enhances the knowledge of the therapeutic

ultrasound effects on compositional cells. This work aims to construct an explanation of the effects of sound waves on the ligament cell's energy absorption capacity evidenced by their elasticity and harmonic vibration. Another goal is to describe the structural modification of the cytoskeleton due to the ultrasound excitation and the relationship with its natural frequencies. The results support that the variation of elasticity and harmonic vibration are dependent on the excitation doses at the cellular level for the healing stages of ligaments. This study contributes to the understanding and provides new elements to comprehend cellular biomechanics.

## 1.2 Materials and Methods

To obtain fibroblasts cells that migrated out of the ligament onto the surface of the dish, an explant culture technique was used (Section 1.2.1). Cells passaging was made in several culture plates to perform both of the experiments, AFM testing and flow cytometer analysis. The design for every single experiment consisted in two different stimulated groups stimulated with ultrasound energy every 24 hours for five days, Group A, received 1.5 J/cm$^2$ and Group B 5 J/cm$^2$ energy doses according to therapeutic range stimulation in cells, and a control Group C which was not stimulated with ultrasound energy (Section 1.2.2).

To detect cell death after treatment with ultrasound was completed a flow cytometer analysis was performed (Section 1.2.3). To measure the cell elastic modulus (Young's modulus) using the Hook law fundaments an AFM testing was done (Section 1.2.4).

Finally, to elucidate the influence of fibroblast elasticity (from stimulated and control groups) on natural frequencies of vibration of the cytoskeleton a FEM (finite element method) analysis was performed using the eigenvalue extraction method Lanczos (ABAQUS/CAE 6.12.3 software). The elastic modulus (median) and the height (mean) were used as input parameters (obtained in the AFM testing). To represent the internal structure (cytoskeleton) of an adherent cell (ligament fibroblast) an octahedron tensegrity model was used (See Section 1.2.5).

### 1.2.1 Explant technique and cell culture protocol

The ethics committee of the Sciences Faculty of the Universidad Nacional de Colombia approved the protocol that was followed in this work. Initially, the cells were obtained using

the primary explant technique from the lateral collateral ligaments (LCL) of both knees of one adult female Wistar rat following the Henshaw, Attia, Bhargava, and Hannafin protocol (2006) (Henshaw et al. 2006).

The LCL were extracted from both knees and maintained in aseptic conditions on culture medium Dulbecco's Modified Eagle Medium: Nutrient Mixture F-12 (DMEM/F12), Gibco (1:1) (1x) supplemented with 1% antibiotics/antifungal (Gibco-Vitrogen Corporation) and 10% fetal bovine serum (FBS) (Gibco-Vitrogen Corporation). The dissection was made by cutting the femoral and fibular insertions. The ligaments were disposed over T-25 culture flasks with sterile culture medium supplemented. The medium was changed every 48 hours.

The flasks were incubated at 37 ºC in a 5% $CO_2$ atmosphere. The explanted cells migrated around the tissue and were adhered and proliferated over the flasks. After 15 days, the tissue was removed from the flasks. The monolayer cultures were confluent at approximately two weeks. They were detached using 0.025% trypsin (Gibco-Vitrogen Corporation) for five minutes and subcultured on a six-well plate for flow cytometry testing.

They also were cultured on Petri dishes for atomic force microscopy (AFM) indentation. They were maintained in 1 mL and 2 mL, respectively, of supplemented culture medium DMEM/F12 at 37 ºC in a 5% $CO_2$ atmosphere. The medium was changed every 48 hours. The remaining cells were cryopreserved in a 10% DMEM/F12 culture medium containing 90% FBS and 10% Dimethyl sulfoxide (DMSO).

The explanted cells were washed with Hank's Balanced Salt Solution (HBSS) (Gibco). They were centrifuged at 287 g for 5 min and evaluated under a microscope by the cell shape to ensure the purity of the culture. To verify that the cells shape explanted from the ligaments corresponded to fibroblasts, their nuclei and their bodies were highlighted through the Hematoxilin-Eosin technique during microscopy observations (Karlsson et al. 2009). We followed the laboratory protocol defined by the Laboratorio de Biomiméticos of the Instituto de Biotecnología de la Universidad Nacional de Colombia, which is in agreement with the protocol described by Spitalnik (2015) (Spitalnik 2015).

## 1.2.2 Ultrasound protocol

In this experiment, a standard therapy device “J-Style” (JC-2902[1]) ultrasound transducer was used in order to follow the standard clinical procedures for therapy on ligaments (Warden et al. 2006b).

For each test, the culture plate was placed over the transducer head, on which a layer of sound wave-transmission gel had been previously applied (Figure 1-1). The control group was processed in the same way as stimulated group, but without exposure to ultrasound energy.

Figure 1-1: Experimental design and simulation model for this work.

[1] Building 6. Huafeng Tech Park, Guangtian Road, Luotian Industrial Area, Songgang Town, Bao’an District, Shenzhen, China. Tel:86-755-33180892 Fax:86-755-33180893. Available on https://m.dhgate.com/product/j-style-jc-2902-face-massager-machine-multi/393944536.html

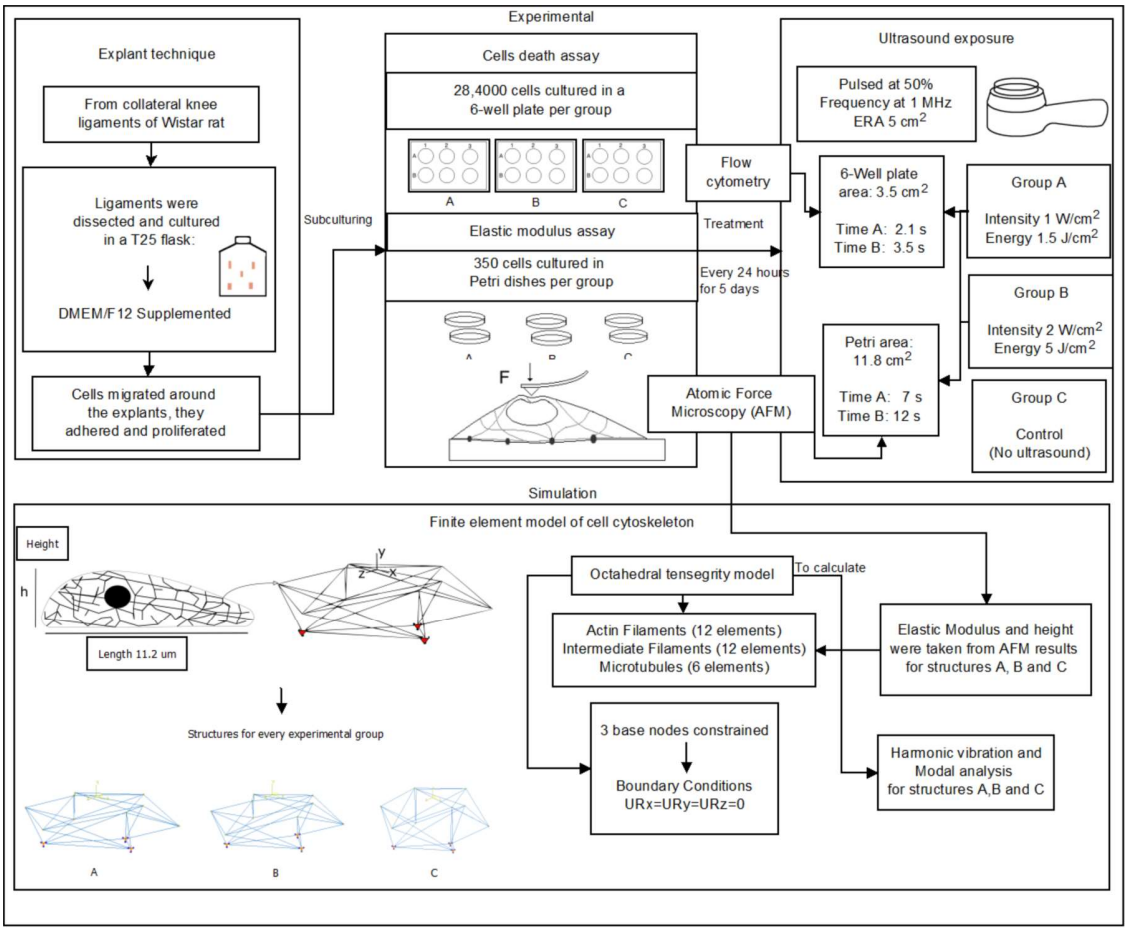


The stimulation was performed in accordance with the frequency of treatment used in physical rehabilitation and the experimental protocol used by Harle et al. (2001) every 24 hours for five days (Carrer et al. 2015; Harle et al. 2001a) under the parameters presented in Table 1-1 at a frequency of 1.0 MHz, which is one of the therapeutic frequency used to treat the ligament injuries (Ng et al. 2003; Uhlemann et al. 2003), in pulsed mode at 50% duty cycle, effective radiation area (ERA) of 5 $cm^2$, spatial average temporal average (SATA) intensity of 0.5 $W/cm^2$, and an intensity of 1.0 $W/cm^2$ for each stimulated group.

Stimulated Group A received an intensity of 1.0 $W/cm^2$ and an energy dose of 1.5 $J/cm^2$, while stimulated Group B received an intensity of 2.0 $W/cm^2$ with an energy dose of 5 $J/cm^2$. The ultrasound parameters for each group, application time and surface area of the plate culture are shown in Table 1-1.

Table 1-1: Ultrasound parameters applied to each treatment group.

| Ultrasound Parameters | | Group A | Group B | Group C |
|---|---|---|---|---|
| Frequency (MHz) | | 1 | 1 | 0 |
| Energy [e] (J/cm$^2$) | | 1.5 | 5 | 0 |
| Intensity [I] (W/cm$^2$) | | 1 | 2 | 0 |
| Effective Radiation Area [$a_t$] (cm$^2$) | | 5 | | |
| SATA (Spatial Average Temporal Average Intensity) (W/cm$^2$) | | 0.5 | 1 | - |
| Duty cycle [D] | | 0.5 | | - |
| Surface area of the plate culture [$a_c$] (cm$^2$) | 6-Well plate: | 3.5 | | |
| | Petri dish: | 11.78 | | |
| Time (s) | 6-Well plate: | 2.1 | 3.5 | - |
| | Petri dish: | 7 | 12 | - |

For these experiments, 5% and 17% of the energy applied to humans was employed based on 30 J/cm$^2$; these values were taken from the therapeutic range proposed in the literature (Bjordal et al., 2007; Baker, Robertson, & Duck, 2001).

According to the ultrasound parameters and the surface area of the plate culture, the application time ($t$) for the ultrasound was calculated utilizing the potency equation to transmit energy at 1.5 J/cm$^2$ and 5.1 J/cm$^2$ to cells for every stimulated Group A and B, See Equation (1-1) (Tole, 2005; Rodríguez, 2008; Baker et al., 2001).

$$t = \frac{e \cdot a_c}{I \cdot a_t \cdot D} \tag{1-1}$$

Where ($e$) is energy per square centimeter, ($I$) is transducer intensity, ( $a_t$) is ERA, ($D$) is duty cycle, and ($a_c$) is cultured area.

### 1.2.3 Flow cytometry

Conjugated annexin V-FITC combined with the cationic marker propidium iodide (PI) was employed to detect non-apoptotic cells, in early apoptosis, necrotic cells, and cells in late apoptosis after treatment (every 24 hours for 5 days). We selected this assay to assess if the external stimulus can trigger phosphatidylserine translocation (assumed to be an early feature of programmed cell death) by Annexin-V, and propidium iodide staining (Span et al. 2002). The samples were analyzed using a flow cytometry system (BD FACSCanto II) with a solid state (L1) laser and a blue (488-nm excitation line, air-cooled, 20-mW solid state), from the Pharmacy Department of the National University of Colombia.

A total of 2.84 x $10^4$ cells were cultured in every six-well plate per group (Figure 1-1) to obtain 100% confluence on the sixth day (when the treatment has finished). One well was stained with fluorochrome annexin V-FITC, another with PI, and another with both. The other wells served as controls. The samples were placed in cytometry tubes suspended in a 300 µL culture medium. Each well corresponded to a specific sample. Ten thousand test runs were performed to identify non-apoptotic cells (Q3:annexin V-FITC negative/PI negative), cells in early apoptosis (Q4:annexin V-FITC positive/PI negative), necrotic cells (Q1:annexin V-FITC negative/PI positive), and cells in late apoptosis (Q2:annexin V-FITC positive /PI positive) (Hingorani et al. 2011).

### 1.2.4 Atomic force microscopy (AFM)

Three hundred and fifty fibroblasts were cultured in Petri dishes (3.5-cm diameter) for every group (exposure to ultrasound energy.

Figure 1-1) to reach 20-40% confluence on the sixth day. All measurements of the cell elastic modulus were performed on proliferating viable cells maintained in culture medium DMEM/F12 within 2-3 hours. The cell elastic modulus was measured using AFM at the University of Los Andes (MFP3D-Bio AFM system (Asylum Research, Santa Barbara, CA)).

We used a pyramidal AFM tip due it is “particularly useful to probe fine features such as the cytoskeleton” (Chen 2014), and “because the magnitude of indentation into the cell is relatively small (<400 nm) compared with the height of the cell where it is probed, the elastic resistance to indentation reflects the stiffness of the cortical actin network” (Solon et al. 2007). Therefore, it was estimated a change of the elastic modulus in the whole cell. This measure was compared with those control samples and stimulated ones, in order to detect significant differences in elastic modulus. Soft cantilevers T R400P B (Olympus, Japan) with a nominal spring constant of 0.09 N/m and tip radius of 42 nm were used. The relative trigger force employed was 2 nN.

The elastic modulus as a function of position on the cell was estimated using the force-volume (F-V) technique by measuring cantilever deflection. To make easier to position the AFM tip a precise location over the cell we used video microscope. The probe moves up and down registering simultaneous the force curve and the cell topography at each pixel of the surface. When the force curve is recorded, at first, the probe is displaced up, and then in the lateral direction to the next pixel of the surface to stay registering.

We obtained force-volume images with a resolution of 20 x 20 pixels within 30 x 30 $\mu m^2$ scan area. The approximate acquisition time per image was 15 minutes. Ten cells per group (A, B, and C) (exposure to ultrasound energy.

Figure 1-1) were measured. The number of effective measurements performed on the A, B, and C groups (Figure 1-1) was 863, 866, and 338 indentations, respectively. We used a larger sample to better determine the average values of the elastic modulus and avoid errors from the indentation depth. Force curves were analyzed from a relative area above the whole cell.

Since elastic modulus calculated from Sneddon Model has dependence of the depth indentation (Guz et al. 2014), and “to nullify the bottom substrate effect in conical tip indentation on the finite thickness” of adherent cell, the asymptotical correction model was used for rigid cone indenting using Equation 1-2 (Managuli and Roy 2018).

$$F_e = \frac{8}{3}\frac{E}{\pi} tan(\theta)\delta^2 \left\{1 + C\frac{4}{\pi^2}\frac{\delta}{h} + C^2\frac{20}{\pi^4}\frac{\delta^2}{h^2} + 0\left(\frac{\delta^3}{h^3}\right)\right\} \quad (1\text{-}2)$$

Where $\mathrm{F}_e$ is the elastic force, $E$ is the elastic modulus, $\delta$ is the indent depth, $\theta$ is the rigid cone angle, which is set to 45º, $\mathrm{h}$ is the thickness of adherent cell at the point of indentation, which is set to 150 nm, 0 represents higher order terms in the series, which is assumed to be negligible, and $C = 1.7795\tan(\theta)$ (Managuli and Roy 2018).

## 1.2.5 Harmonic vibration and modal analysis

To elucidate and simulate the harmonic vibration of the cytoskeleton a FEM (finite element method) analysis was performed using the eigenvalue extraction method Lanczos (ABAQUS/CAE 6.12.3 software). The modal analysis was used to predict the fifth natural frequencies and eigenforms of cytoskeleton for every stimulated Group A and B and control Group C without external excitation. “The mode shapes and natural frequencies provided information concerning what form and with which frequency the structure oscillates freely on the sole basis of its mass and stiffness as well as under defined fixation conditions” (Geltmeier et al. 2015).

To represent the internal structure (cytoskeleton) of an adherent cell (ligament fibroblast) for representing the three configurations of the stimulated groups (A and B) and the control group (C) an octahedron tensegrity model and twelve 3D coordinates to represent the nodes of the structure were used. The cytoskeleton consisted of an octahedron tensegrity network of 30 beam elements (Ingber 2003) (Figure 1-1), which represented twelve actin filaments, twelve intermediate filaments, and six microtubules. They were selected according to the position showed in fluorescence microscopy. The actin filaments were in the cortex, the intermediate filaments in the middle of the structure and the microtubules were in the center (Alberts et al. 2002; Ananthakrishnan et al. 2006).

The mean height values for each cytoskeleton configuration A, B, and C in the simulation were taken from AFM force/volume topography maps. The 100% of the height was input in the Y axes for two node coordinates, and it was adjusted to the 50% height (four node

coordinates), 25% height (two node coordinates) and 75% height (two node coordinates) the other values were zero to maintain the octahedral structure.

The X and Z axes values were taken from literature to comply with the spread shape of the cell (Chen, Wu, Tang, Huang, & Su, 2010) with the 100% length of the cell contact diameter (22.4 μm) (Mcgarry and Prendergast 2004) for two node coordinates, 50% length for four node coordinates, 75% length for two node coordinates, 25% length for two node coordinates and the other values were zero. See supplementary material (Appendix A).

AFM have reported to show the changes in cytoskeleton elastic modulus (Chen, 2014; Hoh & Schoenenberger, 1994), hence, the elastic modulus median values for Groups A, B, and C were taken from the AFM results as input parameters for the elastic modulus in order to calculate the harmonic vibration and the modal analysis for every cytoskeleton configuration. The data for the Poisson's ratio, length, and the beam radius were taken from available literature. These values are provided in Table 1-2 (Jacobs, Huang, & Kwon, 2012; Ofek, Wiltz, & Athanasiou, 2009; Guilak, Haider, Setton, Laursen, & Baaijens, 2006; Mcgarry & Prendergast, 2004).

Table 1-2: Cytoskeleton filament material characteristics. The elastic modulus and the height were taken from the AFM results obtained for Groups A, B, and C. Poisson's ratio, length, and the beam radius were taken from literature.

<table>
<tr><th rowspan="2">Filament</th><th colspan="3">Median elastic modulus (Pa) from AFM</th><th colspan="3">Mean height (μm) from AFM</th><th colspan="3">Length contact radius (μm)</th><th colspan="3">Poisson's Ratio</th><th colspan="3">Beam Radius [m]</th></tr>
<tr><th>A</th><th>B</th><th>C</th><th>A</th><th>B</th><th>C</th><th>A</th><th>B</th><th>C</th><th>A</th><th>B</th><th>C</th><th>A</th><th>B</th><th>C</th></tr>
<tr><td>Actin</td><td rowspan="2">1085</td><td rowspan="2">970</td><td rowspan="2">1399</td><td rowspan="2">4.6</td><td rowspan="2">3.1</td><td rowspan="2">2.7</td><td colspan="3" rowspan="2">11.2</td><td colspan="3">0.4 ± 0.08</td><td colspan="3">$2x10^{-9}$ (Mcgarry and Prendergast 2004)</td></tr>
<tr><td>Intermediate Filaments</td><td colspan="3">0.5 ± 0.05</td><td colspan="3">$5x10^{-6}$</td></tr>
</table>

| | | | | | | | | | |
|---|---|---|---|---|---|---|---|---|---|
| | | | | | | | | | (Guilak et al. 2006) |
| Microtubules | | | | | | | | 0.36 ± 0.06 | $8x10^{-9}$ (Mcgarry and Prendergast 2004) |

The units were converted to micro scale. The cytoskeleton filaments were considered isotropic and elastic since the cells had small deformations 2-8% (Ananthakrishnan et al. 2006; Mcgarry and Prendergast 2004; Palmer and Boyce 2008; Unterberger et al. 2013). The beam length of the contact radius in the tensegrity structure was 11.2 µm (Mcgarry and Prendergast 2004). The density of the filaments was $1.15x10^{-6}$ µg/µm$^3$ (Geltmeier et al. 2015). The initial boundary conditions were imposed on the three base nodes of the tensegrity structure in accordance with the McGarry and Prendergast Model (2004) (Mcgarry and Prendergast 2004) (Figure 1-1). The three receptor nodes represented the focal adhesion of the cell to the extracellular matrix. They were constrained for the three degrees of freedom (U1 = U2 = U3 = UR1 = UR2 = UR3 = 0).

## 1.3 Results

### 1.3.1 Fibroblasts isolated from the LCL

Figure 1-2 shows fibroblasts isolated from the LCL of one adult female Wistar rat under Hematoxylin-Eosin staining which highlights typical characteristics of a cell identified as a fibroblast, such as the nucleus and body, the flat, elongated and triangular shape. “They link fibroblasts into the characteristic meshwork, which is one of the ways they are recognized to be fibroblasts” (Abercrombie 1978).

Figure 1-2: Fibroblasts explanted from the LCL in the knee and stained in Hematoxylin-Eosin.

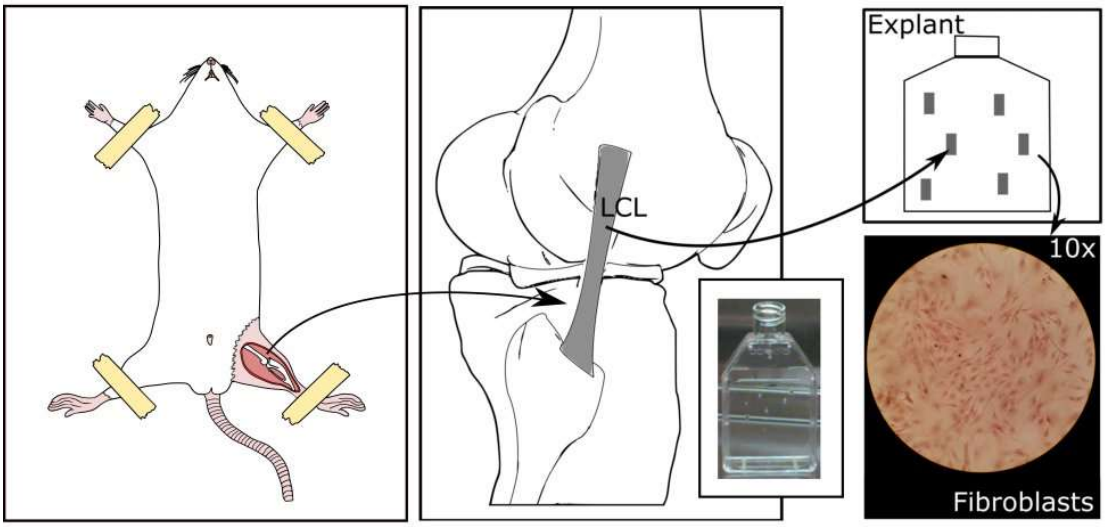


## 1.3.2 Cell death

Figure 1-3 shows the histograms from the cellular death test, which represent the number of cells that emitted fluorescence intensity for each annexin fluorochrome FITC and PI application. For stimulated groups (see Figure 1-3A, Figure 1-3B) and the control group (see Figure 1-3C). The number of events was 10,000. Figure 1-4 shows the bar plot for the mean number of events for the three groups (A, B, C) for each region.

Figure 1-3: Histogram and dot plot density. Results of the membrane alteration cell death test with fluorescein conjugated annexin V-FITC combined with the cationic marker propidium iodide (PI) and detection using flow cytometry. From top to bottom, the results are presented for groups A, B, and C. Noted in each region are Q1: necrotic cells; Q2: late apoptosis; Q3: viable cells; and Q4: cells in early apoptosis.

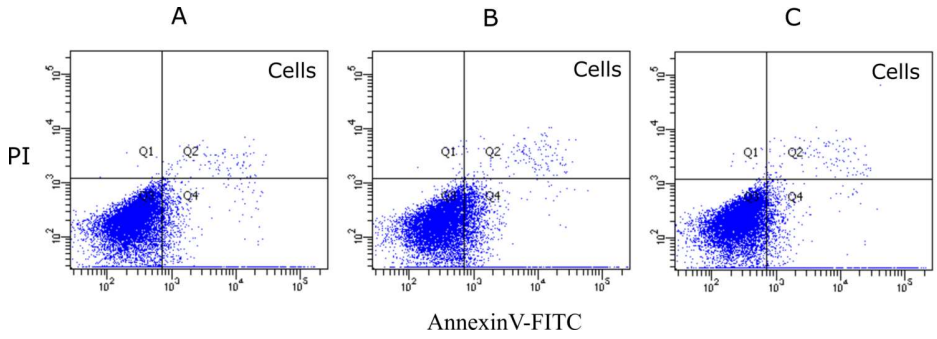


Figure 1-4: Bar plot for the mean number of events for the three groups (A, B, C) for each region from the data generated by flow cytometry. (Q1: necrotic cells; Q2: late apoptosis; Q3: viable cells; and Q4: cells in early apoptosis)

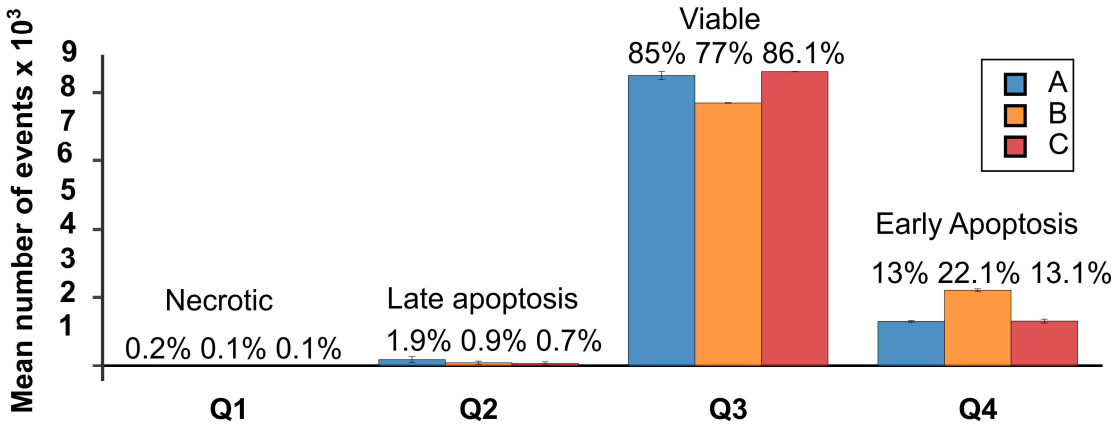


For each region from the data generated by flow cytometry (Necrotic cells (Q1), Late apoptosis (Q2), Viable cells (Q3), Early apoptosis (Q4)) for stimulated Groups (A and B) and control Group (C), statistical analysis was analyzed. Significant differences were not found among the groups. We interpreted there is no dependence between the level of energy and intensity of the ultrasound and the cell death. See supplementary material (Appendix B).

### 1.3.3 Elastic Modulus

In both treatment Groups (A and B) exposed to doses of therapeutic ultrasound which had an elastic modulus (median) of 1085 Pa for the group stimulated with an intensity of 1.0 W/cm2 (Group A) and an elastic modulus (median) of 970 Pa for the group stimulated with an intensity of 2.0 W/cm2 (Group B), the elastic modulus (median) was lower than in the control group that had an elastic modulus (median) of 1399 Pa. Group B had the lowest elastic modulus. Descriptive statistics for each group can be observed in Table 1-3.

Table 1-3: Descriptive statistics for the elastic modulus for treatment Groups A and B, and the control Group C.

| Descriptive Statistics Summary | Group A | Group B | Group C |
|---|---|---|---|
| Length | 863 | 866 | 338 |
| Mean [Pa] ± SD | 1303.1 ± 797.1 | 1119.3 ± 634.5 | 1653.0 ± 965.0 |
| Median [Pa] | 1085 | 970 | 1399 |
| Q1 | 722 | 665 | 1049 |
| Q3 | 1710 | 1392 | 1964 |
| Min | 174 | 233 | 181 |
| Max | 4877 | 3751 | 4848 |

Figure 1-5 shows in comparative form the elastic modulus calculated using the AFM technique. Greater dispersion was observed for the control group, as compared to the stimulated groups.

Figure 1-5: Elastic modulus trend and distribution of the treatments (A and B) and control group (C).

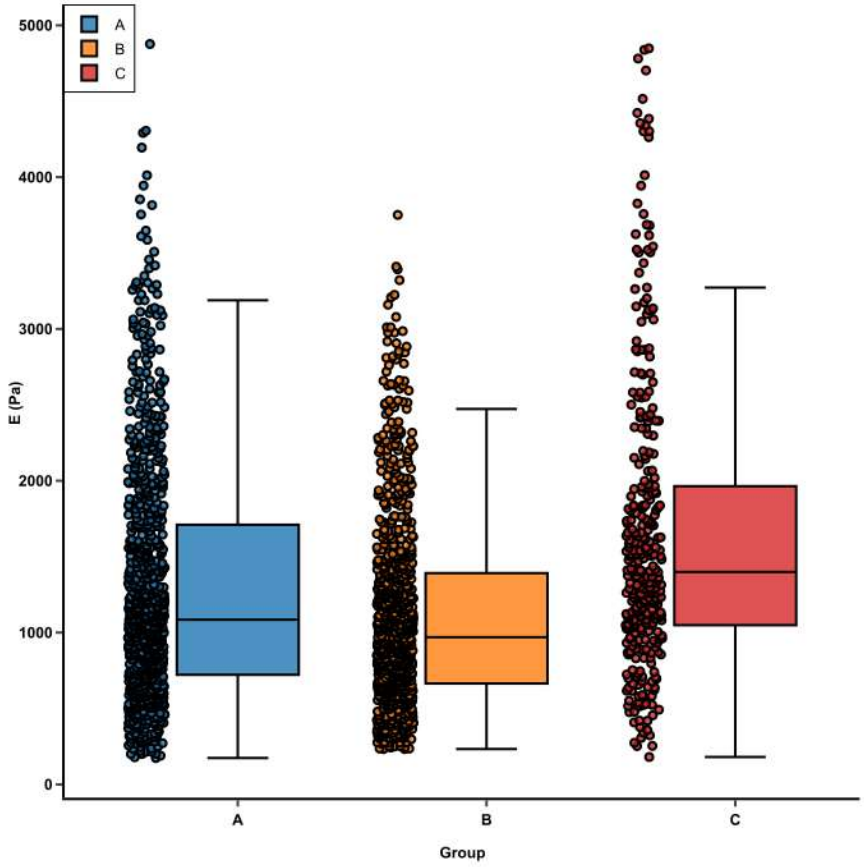


The three-dimensional (3D) force/volume topography maps show the volume of the cell and its relation to the elastic modulus (Figure 1-6). The darker the color of the cell, the lower the elastic modulus. Cells from stimulated Group A (Figure 1-6A) had a mean height of 4.6 µm. Cells from stimulated Group B (Figure 1-6B) had a mean height of 3.1 µm and a lower elastic modulus. Cells from the control group (Figure 1-6C) had a mean height of 2.7 µm and showed a higher elastic modulus.

Figure 1-6: 3D strength/volume topography maps using AFM. The darker the color of the cell, the lower the elastic modulus.

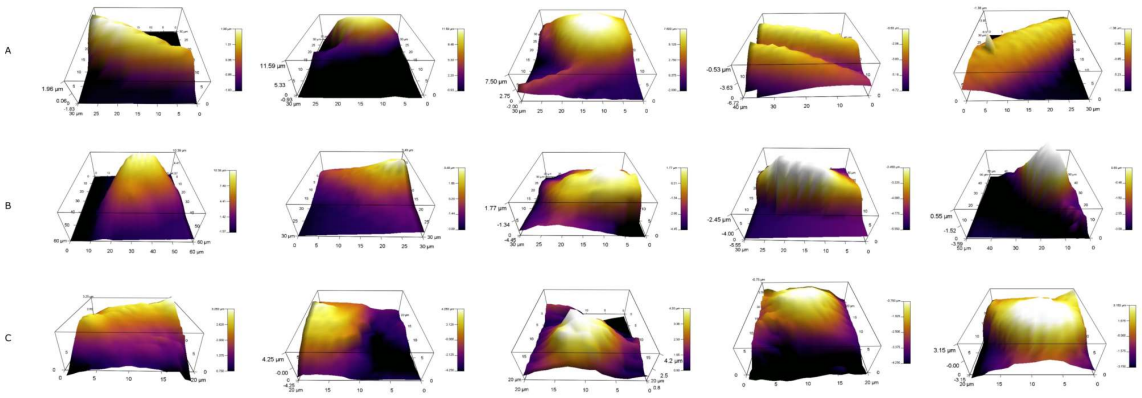

In the statistical analysis (non-parametric statistical test of Kruskal-Wallis) significant differences ($p \leq 0.05$) were found among the different experiment groups. We interpreted there is dependence between the level of energy and intensity of the ultrasound and the elastic modulus. See supplementary material (Appendix C).

## 1.3.4 Harmonic vibration and modal analysis

Figure 1-7 graphically presents similar displacements of the cell structure for five harmonic vibration frequencies and modes for stimulated A and B, respectively (see Figure 1-7A and Figure 1-7B) and control Group C (see Figure 1-7C). It also has been shown for fiftieth vibration modes for all groups (see Animations 1, 2 and 3).

Figure 1-7: Cytoskeleton structure deformation (μm) for each treatment (A and B) and control group (C). Maximum deformation ($1x10^0$) and minimum ($0x10^0$).

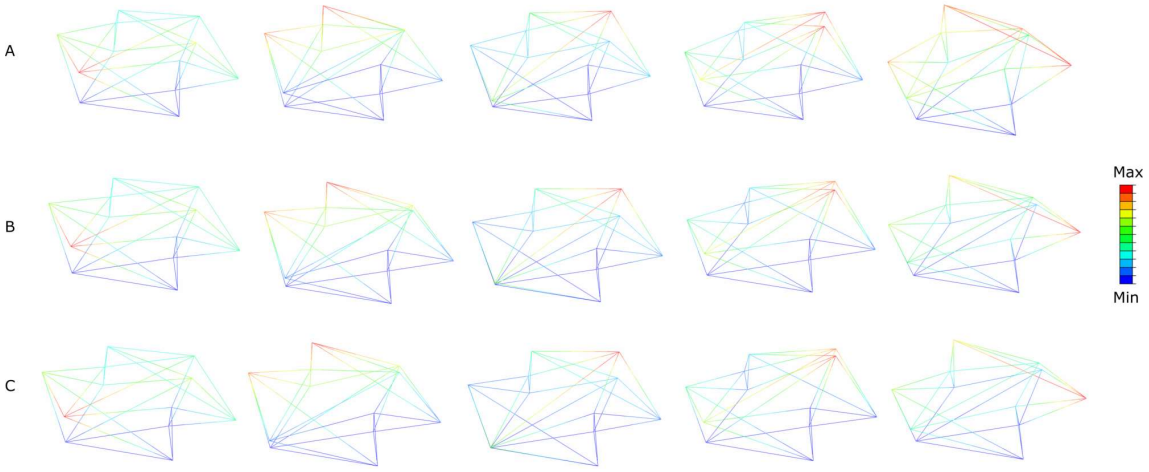


In Figure 1-8, we present the natural vibration frequencies for three configurations of cell structure. Every configuration corresponds with Group A, Group B, and Group C, respectively, and takes the elastic modulus (median) and the height (mean) obtained from the AFM test (see Table 1-1). The figures show that there are higher frequencies of vibration when the elastic modulus is higher (Group C), reaching a maximum vibration frequency of $4.1 \times 10^9$ Hz at the fifth vibration mode. When the cytoskeleton filaments have the elastic modulus of Groups A and B from the AFM results, the vibration frequencies decrease to a maximum of $3.3 \times 10^9$ Hz at the fifth vibration mode.

**Figure 1-8:** Natural frequencies of vibration for each treatment (A and B) and control group (C).

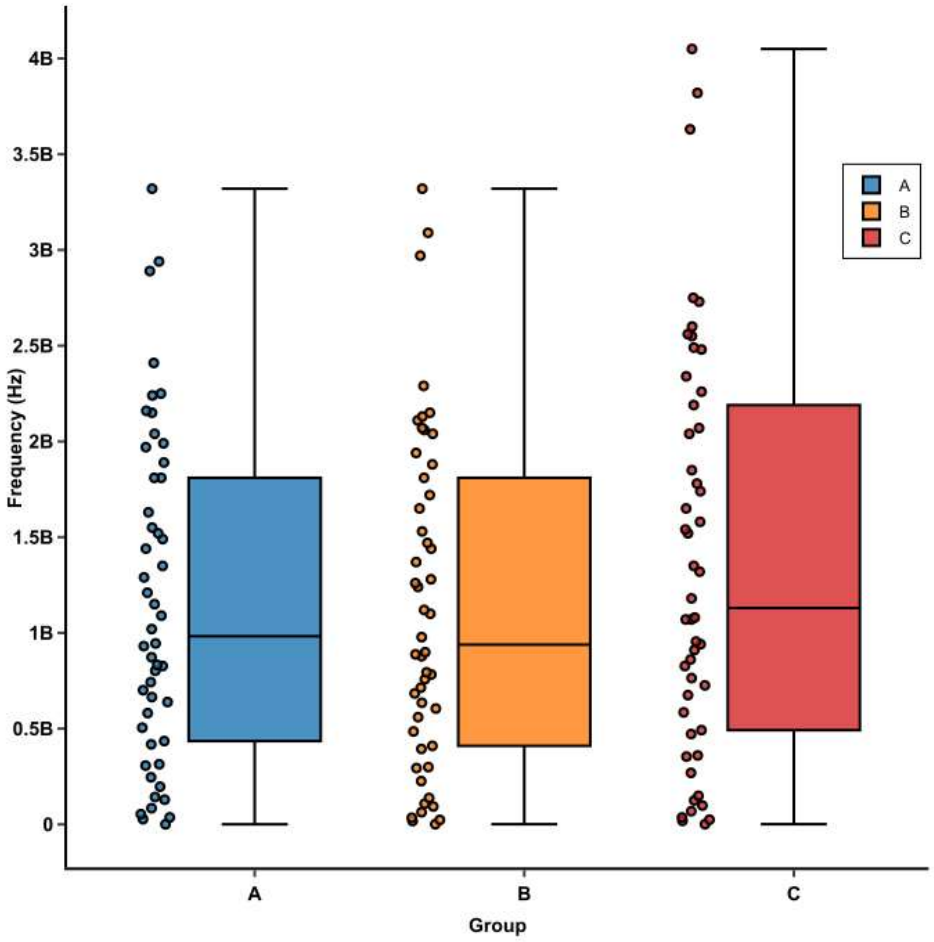


## 1.4 Discussion

In this study, we have shown that the elastic modulus of fibroblasts isolated from LCL significantly decreased 22% and 31% owing to the application of pulsed therapeutic ultrasound at 1.0 MHz with intensity doses of 1.0 W/cm$^2$ and 2.0 W/cm$^2$, respectively. We have used the statistical median to compare the elastic modulus (Codan et al. 2013), and demonstrated significant differences among the different experiment groups.

We note that our experimental elastic modulus results were higher than values for fibroblasts with decreased adherence, 0.6 ± 0.1 kPa (Mahaffy et al. 2004), and they were in a range of a typical values for fibroblasts, 1 to 5 kPa (Codan et al. 2013; Simon and Durrieu 2006; Solon et al. 2007). Here, the elastic modulus reflects the resistance to

indentation tip of the cortical actin network (Solon et al. 2007). The high standard deviation may be explained by the variant configuration of the cell membrane mesh and its heterogeneous surface (Kuznetsova et al. 2007).

We hypothesize that cells stimulated with therapeutic ultrasound decreased their elastic modulus to promote cell motility due cross-linked network of actin filaments that are perturbed and focal adhesions as well (Stricker et al. 2010). According to Swaminathan et al. (2011), the cells have to reorganize their cytoskeleton in order to move through the extracellular matrix which produces a decrease in the elastic modulus of the cell (Swaminathan et al. 2011). This also may explain the shape changes observed in the cell force/volume maps and the decreased elastic modulus of the stimulated cells in our study. This phenomenon occurs biochemically by the assembling of the cytoskeleton network to facilitate cell motility (Michalczyk & Ziman, 2005; Ananthakrishnan et al., 2006), likewise cell migration (Roper et al. 2015).

Thus, we can hypothesize that the elastic modulus decreased owing to the assembling of the actin filaments in the leading edge of the cell to prepare the cellular motility (Haase et al. 2015; Pollard and Borisy 2003), and it is not related to cell death (Pozzi et al. 2011). This was also shown through cell death testing. In stimulated Group A or Group B, most of the cell remained viable at 86% and 77%, respectively. These cell death results differ from another study that showed an increased number of cells suffering an apoptotic reaction when treated with ultrasound. It can be explained due the higher energy density (600 $W/cm^2$) and frequency (4.36 MHz) used in that study over human colon adenocarcinoma cell line (HT29) (Schuster et al. 2013).

We also revealed the modes and frequencies of vibration of the cell cytoskeleton by numerical analysis using the elastic modulus (median) and the height (mean) obtained in the AFM testing. We found that, while the elastic modulus of the filaments was higher, as was the elastic modulus obtained in the AFM testing for the control group (C), harmonic vibration frequencies were also increased by the time as it has been showed in cells (Jaganathan, Saravana Kumar Subramanian et al. 2016). Geltmeier et al. (2015) showed similar results; they concluded that the natural frequencies of the normal cells were higher owing to their high elastic modulus (Geltmeier et al. 2015).

We predicted frequencies of vibration of 402 kHz (1st vibration frequency), in a range between 27.2 MHz to 945 MHz for the first twentieth fifth vibration frequencies for treatment Group A; 806 kHz (1st vibration frequency), in a range between 17.5 MHz to 978 MHz for the first twentieth sixth vibration frequencies for stimulated Group B, and the last frequencies of vibration estimated for both stimulated groups were in a range between $1x10^9$ Hz to $3.3x10^9$ Hz until the fiftieth vibration frequency.

We also predicted frequencies of vibration of 983 kHz (1st vibration frequency), in a range between 18,3 MHz to 955 MHz for the first twentieth second vibration frequencies for control Group C, and the last frequencies of vibration estimated were in a range between $1x10^9$ Hz to $4.1x10^9$ Hz until the fiftieth vibration frequency.

This means the cytoskeleton frequency of non-stimulated cells was found to be 20% higher than cytoskeleton of stimulated cells for the last frequency of vibration, and it may explained due to higher dimensions and higher elastic modulus of the cytoskeleton for control group.

While we only calculated the natural frequencies of vibration of the cytoskeleton for the treatment and control groups without considering other elements of the cell like the cytosol and the nucleus, we suggest more computational models to hypothesize the chance to cause resonant effect using therapeutic ultrasound with a frequency of 1.0 MHz.

We demonstrated at the cellular level that the cell elasticity and the cytoskeleton harmonic vibration is significantly dependent upon the frequency and the energy density applied. For low frequency and low-pulsed energy density, therapeutic ultrasound might be used to increase and stimulate ligament healing.

# 2. Non-thermal effect of therapeutic ultrasound on cell cultures

## 2.1 Introduction

Ultrasound is a high frequency acoustic mechanical wave inaudible to human beings in which energy is transmitted by molecules that collide in a conductive medium, and that produces vibration and a minimum displacement of other adjacent molecules that can cause either thermal or non-thermal (mechanical) effects (Draper and Prentice 2011).

Ultrasound is one of the most commonly employed therapeutic modalities in physical rehabilitation. It is used primarily to stimulate cells that repair tissues and produce greater extracellular matrix, which leads to greater mechanical resistance in the tissue (Knight and Draper 2013).

Continuously applied ultrasound produces heat due to the energy transmitted between the molecules of the biological medium. Vitro methodology is used to understand this phenomenon at cellular levels. When an ultrasound beam passes through a cell culture, some acoustic pressure field energy is transformed into heat as it is absorbed locally by the culture. This attenuation is caused primarily by processes of absorption, scattering and beam deflection, which convert ultrasound energy into heat (Draper and Prentice 2011).

Ultrasound that is applied in a pulsed manner will produce mechanical effects rather than thermal effects. (Lennart 2002). In vitro studies show that the increase in cell culture temperature is lower than 0.5ºC when the frequency of ultrasound is 1 or 3 MHz. The application is 5 to 10 minutes long and pulsatile (Bohari 2011; Lennart 2002).

This mechanical effect is due to the combination of streaming and stable acoustic cavitation. Streaming corresponds to the physical force produced by the wave capable of displacing ions organelles and small molecules (Lennart 2002). Acoustic cavitation results from the rapid changes in pressure produced by the sound wave, which generates tiny

vacuum bubbles that contract and expand in the liquid microenvironment without collapsing (Lennart 2002).

The effectiveness of ultrasound depends on the medium's physical properties (acoustic absorption coefficient, density and specific heat), the properties of the ultrasound device (beam geometry), the frequency, the average time of sound field intensity and the modality applied (thermal or mechanical). For therapeutic cases, the intensity is in the range of 0.5-2.0 W / cm2 (Cambier et al. 2001), energy is between 30 -11,600 Joules (Robertson and Baker 2001), and the continuous application is contraindicated due to the thermal effects produced in cases of edema, acute inflammation, infection, hemorrhages and coagulation problems.

Although studies on humans raise questions about its efficiency in relieving pain (Draper & Prentice 2011; Van Den Bekerom et al., 2011), studies on rats have shown rapid cell proliferation and acceleration of tendon regeneration (Schencke & del Sol 2010). However, there is still no consensus on the dose of ultrasound required to mechanically stimulate the cells without producing thermal effects (De Deyne and Kirsch-Volders 1995; Louw et al. 2013).

Mathematical models related to the propagation of acoustic waves are helpful in understanding this phenomenon. Numerical implementation represents in a useful and realistic way the therapeutic application of ultrasound at the cellular and tissue level. Particularly, the Helmholtz equation has been used to represent the linear wave equation with time-dependent harmonic oscillation and to understand the effect of low intensity ultrasound on chondrocyte cultures (Louw et al. 2013).

For the reasons stated above, this paper uses both experimental in vitro and computational models to determine the acoustic pressure, temperature change and internal energy produced in a cell culture of fibroblasts exposed to two doses of therapeutic ultrasound. The objective is to demonstrate that ultrasound applied in two therapeutic doses does not produce thermal changes in fibroblast cell cultures.

## 2.2 Materials and Methods

An in vitro experiment was carried out, which consisted of triplicate cell cultures for each treatment groups (A, B and control group C). Thereafter, ultrasound treatment was

employed. The temperature of the cell culture was measured before and after the treatment. Lastly, the experiment was modeled and simulated in the COMSOL software to estimate the acoustic pressure and temperature. The methodology is explained in detail in what follows.

## 2.2.1 Cell Culture

The cell culture was created using a cell line of 3T3 mouse embryonic fibroblasts in the National University of Colombia's Biomimetics Laboratory, which is part of its Biotechnology Institute. Cells were grown as monolayers in three plastic Falcon Petri dishes measuring 35 mm in diameter and with a cultivation area of 11.78 cm2 for each treatment and control group. As shown in Figure 2-1, the cell culture dish area was fit perfectly over the ultrasound transducer. Cells were maintained with Gibco ™ Dulbecco's modified Eagle Medium culture medium. The F-12 nutrient mixture (DMEM / F -12) was supplemented with Gibco ™ 10% fetal bovine serum and 1% antibiotic / antifungal.

**Figure 2-1:** Therapeutic ultrasound applied to a cell culture

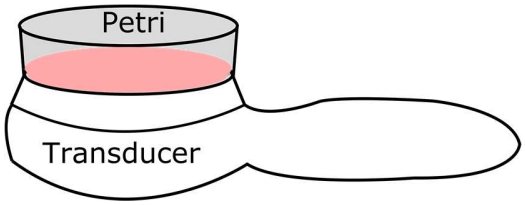


### 2.2.2 Ultrasound

Pulsed ultrasound at 50% at a frequency of 1.0 MHz and ERA measuring 5cm$^2$ were applied to Petri culture boxes. A layer of ultrasonic wave transmitter gel was then applied to prevent wave dissipation. The specific parameters applied to the ultrasound are presented in Figure 2-2. The control group did not receive energy from the ultrasound, and the Petri dish was kept on the transducer for the same length of time as treatment group B.

**Figure 2-2:** Therapeutic ultrasound applied to a cell culture

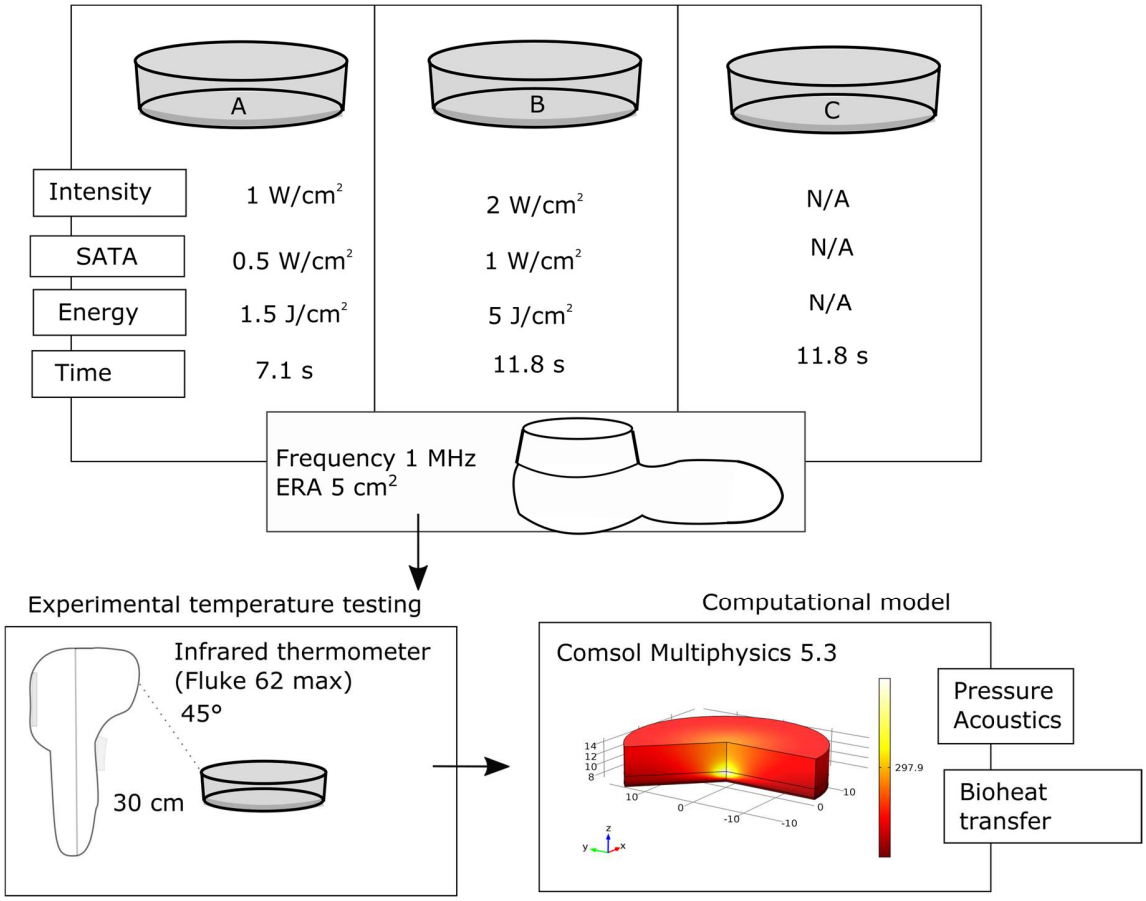


## 2.2.3 Temperature

As shown in the dose presented in Figure 2-2, the culture medium's temperature was measured before and after the ultrasound treatment, using an infrared thermometer (Fluke 62max IR thermometer) from a distance of 30 cm distance and at 45º angle. Triplicate measurements were made for each Petri dish sample. There were four samples for each group.

## 2.2.4 Statistical analysis

Pearson chi-square, Shapiro-Wilk and Kolmogorov-Smirnov normality tests were performed on the pre (A0, B0, C0) and post-treatment samples (A1, B1, C1). None presented the normality condition. The following non-parametric statistical test was

performed on each experiment: Kruskal-Wallis for independent, post-sample samples. The null hypothesis is that the samples are the same. If $p \leq 0.05$, the null hypothesis is rejected (visualization used from BioVinci version 1.1.3 developed by BioTuring Inc., San Diego California USA, www.bioturing.com).

### 2.2.5 Numerical implementation

A linear wave equation mathematical model with time-dependent harmonic oscillation was employed. The model was derived from computational experiments performed to measure the heating of an artificial tissue (tissue phantom) induced by focused ultrasound (COMSOL Multiphysics 5.3 2018). To validate the model, the same COMSOL tutorial simulation was implemented (COMSOL Multiphysics 5.3 2018). The results were the same. Next, the global definitions as parameters, geometry and materials were modified to customize the model to the particular case of exposure of therapeutic ultrasound to a cell culture (See Table 2-1).

### 2.2.6 Geometry

A cylinder-shaped cell culture dish (Petri dish), with a diameter if 35 and a height of 10 mm, was used. The cell culture dish and the transducer were arranged coaxially, and so the model was defined as axisymmetric 2D, as shown in Figure 2-3. The COMSOL Multiphysics 5.2 software was used to simulate the energy transfer of the ultrasound transducer to a monolayer cell culture.

The transducer had a rectangular shape with a radius of 23.5 mm to represent the experimental design. It had a frequency of 1.0 MHz. It was active for 1 second (pulse time "on") and then it was switched off (pulse time "off") according to the duty cycle (50%) of the

experimental design parameters, Table 2-1. This model calculated the heating of the cell culture and the energy of the Petri dish. The acoustic pressure was also calculated.

**Figure 2-3:** Simulated Geometry

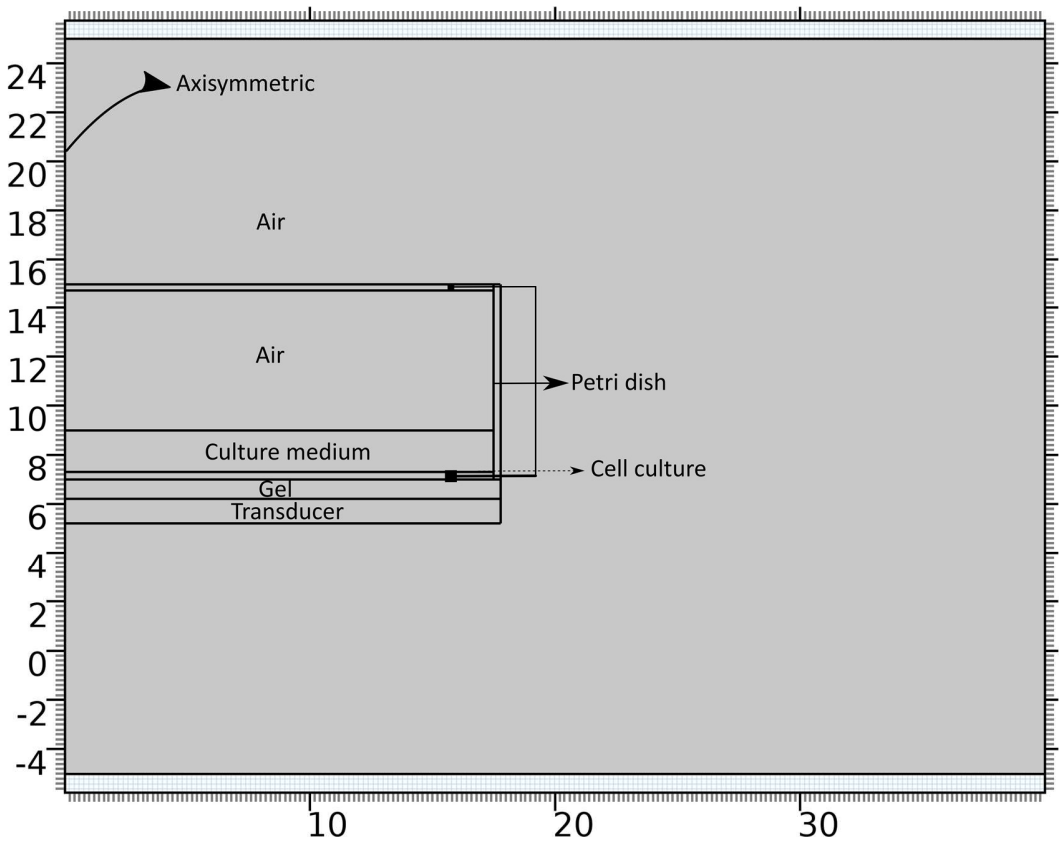


Pressure and temperature were designated as dependent variables. Thermal simulation implementation was limited to the domain of the cell culture and in that of the Petri dish. The simulation of the acoustic pressure was performed in all domains.

The model employed a mesh measuring size λ / 4 (where λ is the wavelength). Fourth-order elements were used to discretize the acoustic pressure and the second-order elements to discretize the temperature. See Figure 2-4.

**Figure 2-4:** Acoustic pressure and temperature mesh in all domains

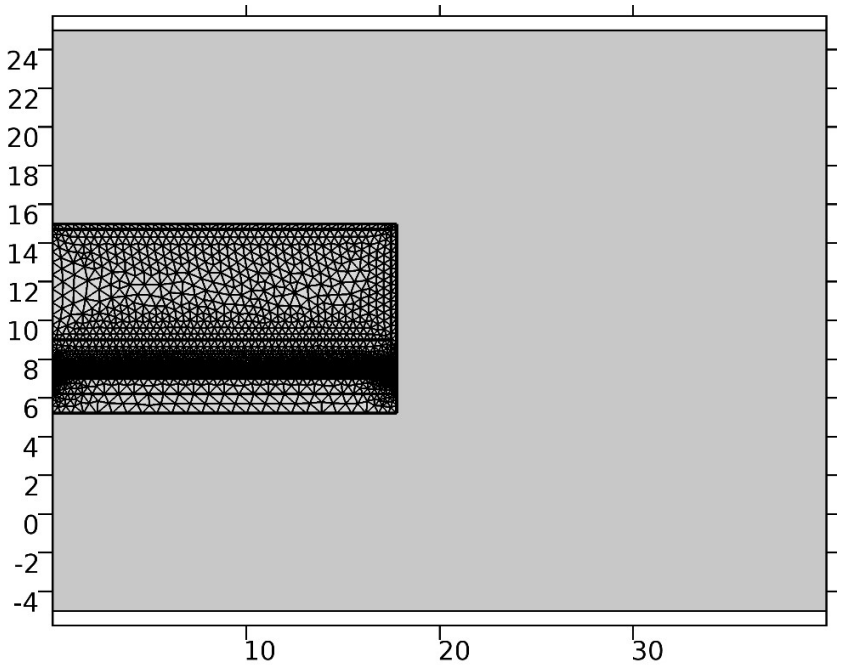


## 2.2.7 Equations

The relevant resolved wave equation was the homogeneous Helmholtz equation for axisymmetric 2D geometry with cylindrical coordinates (COMSOL Multiphysics 5.3 2018):

$$\frac{\partial}{\partial r}\left[-\frac{r}{\rho_c}\left(\frac{\partial p}{\partial r}\right)\right] + r\frac{\partial}{\partial z}\left[-\frac{1}{\rho_c}\left(\frac{\partial p}{\partial z}\right)\right] - \left[\left(\frac{\omega}{c_c}\right)^2\right]\frac{rp}{\rho_c} = 0 \qquad (2\text{-}1)$$

The assumption when employing Equation (2-1) was that the propagation of the acoustic wave was linear and the amplitude of the shear waves in the cell culture domain are much smaller than the pressure waves. That was, since sound waves comply with the principle of linear superposition, acoustic disturbances are small and high-order terms can be neglected (Louw et al., 2013). Nonlinear effects and shear waves are not considered.

The equations assumed for the domain frequency are Equations (2-2) to (2-7):

$$\nabla \cdot \left( \frac{1}{\rho_c} \left( \nabla \rho_t - \mathbf{q}_d \right) \right) - \frac{k_{\text{eq}}^2 p_t}{\rho_c} = \mathrm{Q}_m \tag{2-2}$$

Where

$$p_t = p + p_b \tag{2-3}$$

$$k_{\text{eq}}^2 = \left( \frac{\omega}{c_c} \right)^2 - \left( \frac{m}{r} \right)^2 \tag{2-4}$$

$$c_c = \frac{\omega}{k}, \rho_c = \frac{\rho c^2}{c_c^2} \tag{2-5}$$

For the acoustic pressure in the transducer and medium:

$$k = \frac{\omega}{c} - i\alpha \tag{2-6}$$

For the acoustic pressure in the Petri dish, gel and cells:

$$k = \frac{\omega}{c} - i \ln(10) \frac{\alpha}{20} \tag{2-7}$$

Temperature and absolute pressure were the input variables. In

Table 2-1and Table 2-2, these and other parameters can be observed. The initial values for the pressure and first derivative of the pressure over time were initiated at zero.

Table 2-1. Global parameters

| Property | Value | Description | Reference |
|---|---|---|---|

| | | | |
|---|---|---|---|
| Air absorption coefficient ($\alpha$) | 0.01727 [Np/m] | Air absorption coefficient at 10° C, 12500 Hz, 5% relative humidity | (COMSOL Multiphysics 5.3 2018) |
| Air pressure | 20 [$\mu$Pa] | Air pressure | (COMSOL Multiphysics 5.3 2018) |
| Transducer displacement amplitude | 18.1 [nm] | Calculation derived using the amplitude equation | Calculated Data (Appendix D ) |
| Frequency | 1 [MHz] | Value taken from the ultrasound manufacturer | (JC-2902)[2] |
| Temperature initial value | 297.9[K] | Average value measured by a thermographer[3] | Experimental |
| Cell culture start position | 5[mm] | Value taken from in vitro experimental conditions | Experimental |
| Absolute pressure | 1[atm] | Value taken from literature | (COMSOL Multiphysics 5.3 2018) |

[2] Building 6. Huafeng Tech Park, Guangtian Road, Luotian Industrial Area, Songgang Town, Bao'an District, Shenzhen, China. Tel:86-755-33180892 Fax:86-755-33180893. Available on https://m.dhgate.com/product/j-style-jc-2902-face-massager-machine-multi/393944536.html

[3] Fluke 62 Mini Infrared Thermometer

The boundary condition for the calculation of the acoustic pressure was:

$$-\mathbf{n}\cdot\left(-\frac{1}{\rho_c}\left(\nabla p_t-\mathbf{q}_d\right)\right)=(\mathrm{i}\omega)^2\mathrm{d}_n \tag{2-8}$$

The displacement amplitude value of the transducer was input $\mathrm{d}_n$, see Table 2-1.The following Figure 2-5 shows the contour condition delimitation for the Petri cell culture dish in blue and the transducer with respect to the acoustic pressure in red.

**Figure 2-5:** Contour conditions for acoustic pressure

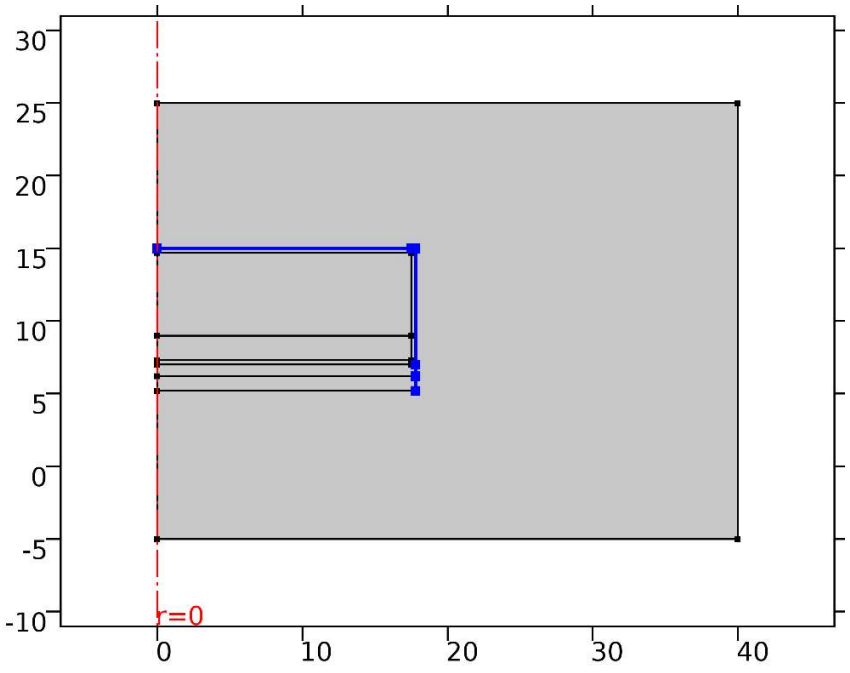


Given the acoustic pressure field, the acoustic intensity field is derived. The heat source Q for the thermal simulation, given at the plane wave limit, was then calculated as (COMSOL Multiphysics 5.3 2018):

$$Q = 2\alpha_{ABS} I = 2\alpha_{ABS} \left| Re\left(\frac{1}{2} p \mathrm{v}\right)\right| \quad (2\text{-}9)$$

Where $\alpha_{ABS}$ is the acoustic absorption coefficient, $I$ was the acoustic intensity magnitude, $p$ was the acoustic pressure, and $\mathrm{v}$ was the acoustic velocity vector. In COMSOL, the intensity was a derived variable where the magnitude can be searched as acpr.I_mah. Additionally, the dissipated power density (for flat waves) was defined as acpr.Q_pw. In this way, the heat source Q can be calculated after the acoustic field was resolved (COMSOL Multiphysics 5.3 2018).

By inserting the volumetric acoustic heat source into the bio-heat transfer equation (heat transfer model for biological tissues) (COMSOL Multiphysics 5.3 2018), we obtain

$$\rho C_p \frac{\partial T}{\partial t} = \nabla \cdot (k \nabla \mathrm{T}) - \rho_b C_b w_b (T - T_b) + Q + Q_{met} \quad (2\text{-}10)$$

Where $T$ es temperature, $\rho$ is density, $C_p$ was specific heat, $k$ was thermic conductivity, $\rho_b$ was blood density, $C_b$ was blood specific heat, $w_b$ was the blood perfusion index, $Q$ es the heat source (the absorbed ultrasound energy calculated in Equation 2), y $Q_{met}$ was the heat source metabolic rate (COMSOL Multiphysics 5.3 2018). In this model it was assumed that crop properties do not change when the temperature increases (COMSOL Multiphysics 5.3 2018).

The temperature calculation for the boundary condition in the Petri dish and in the middle was:

$$-\mathbf{n} \cdot \mathbf{q} = 0 \quad (2\text{-}11)$$

For the cells:

$$T = T_0 \tag{2-12}$$

The temperature value was the input $T_0$, see

Table 2-1.The following Figure 2-6 presents the boundary conditions for the Petri dish in blue and the medium and for the cell culture area in red.

**Figure 2-6** Temperature boundary conditions

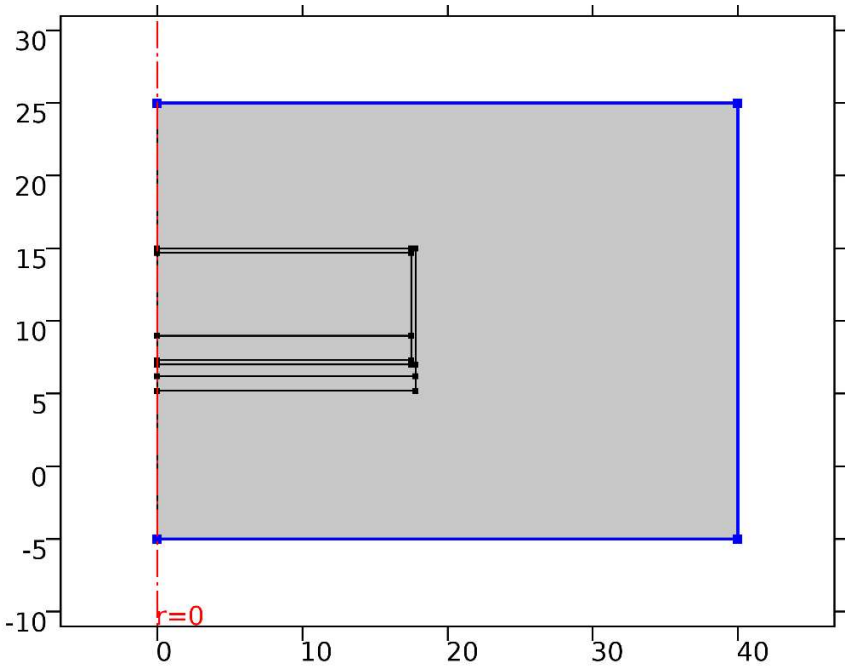


In Table 2-2, the cell culture material properties are observed (Lucia 2015; Park et al. 2016; Pasternak et al. 2015): gel (FDA 2014; Gonzalo-Garijo et al. 2011; Jönsson 2015; Menikou and Damianou 2017) and polystyrene (Algaer 2010; Lochab and Singh 2004; Zhang 2013). The material properties for the air and the culture medium were taken from the COMSOL library, both of which were equivalent to that of water (COMSOL Multiphysics 5.3 2018). The attenuation coefficient for air was 0.01727 dB/m (Harris 1966) and for the medium 0.025 Np/m (COMSOL Multiphysics 5.3 2018).

Table 2-2. Material properties for cell culture, gel, polystyrene, air and culture medium.

| Material properties | Cell culture | Gel | Polystyrene |
|---|---|---|---|
| Density ($\rho$) [Kg/m$^3$] | 993 | 1060 | 1050 |
| Sounds velocity ($c$) [m/s] | 1565 | 1320 | 2450 |
| Thermic conductivity ($k$) [W/m·K) | 0.585 | 0.585 | 0.187 |
| Specific heat at constant pressure ($C_p$) [J/Kg·K] | 4186 | 4186 | 2092 |
| Attenuation coefficient (α) [dB/m] | 1.20 | 0.6 | 1.8 |

## 2.3 Results

Next, presented are the results obtained in the controlled experiment and computational model.

### 2.3.1 Temperature

Because the test data do not comply with the normality principle (Pearson chi-square, One-sample Kolmogorov-Smirnov and Shapiro-Wilk) the nonparametric Wilcoxon test was performed (Wilcoxon rank sum test with continuity correction). Before and after treatment, the level of significance obtained for group A, B and C was 0.47, 0.16 and 0.09, respectively. Since the significance was greater than or equal to 0.05, the null hypothesis is accepted and thus concluded that the pre and post treatment temperature does not change for any of the groups. Figure 2-7 shows a bar chart comparing the average temperature for all groups.

**Figure 2-7**. Bar graph of temperature change for groups, before (A0, B0 and C0) and after (A1, B1 and C1) treatment. Error bas indicate SEMs

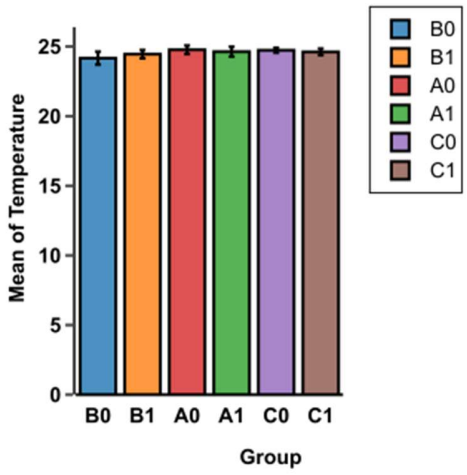


For the three groups, the comparison of post-treatment samples through the non-parametric Kruskal-Wallis test yielded a level of significance of 0.216. Because the significance was greater than 0.05, the null hypothesis was accepted and it was concluded that the temperature was the same for the three treatment and control groups (A1 = B1 = C1). Therefore, the therapeutic ultrasound applied in the dose presented for groups A and B does not produce significant changes in temperature.

## 2.3.2 Simulation

Figure 2-8 shows the acoustic pressure produced in relation to the longitude geometry. The highest pressure peak was received by the medium (810 Pa). These values were exported from the software.

**Figure 2-8**. Simulated geometry acoustic pressure field

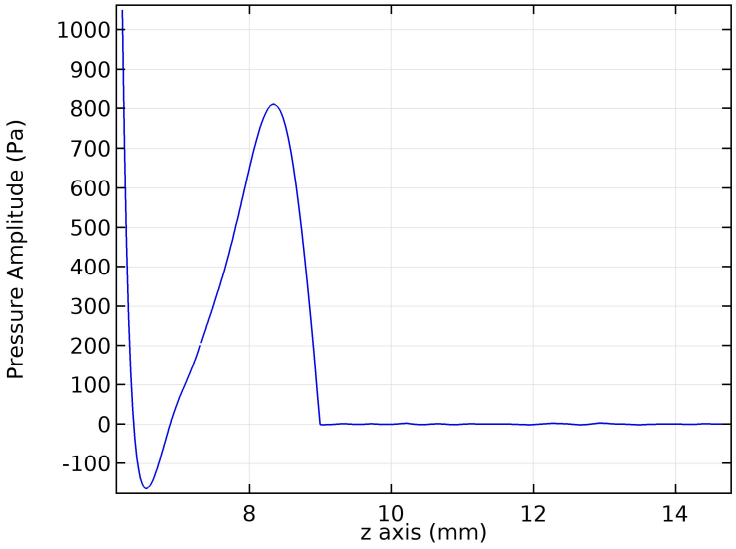


Figure 2-9 shows the acoustic pressure in 3D. The ultrasound beam travels through the gel, cell culture, and culture box.

**Figure 2-9:** Gel and cell culture acoustic pressure fields

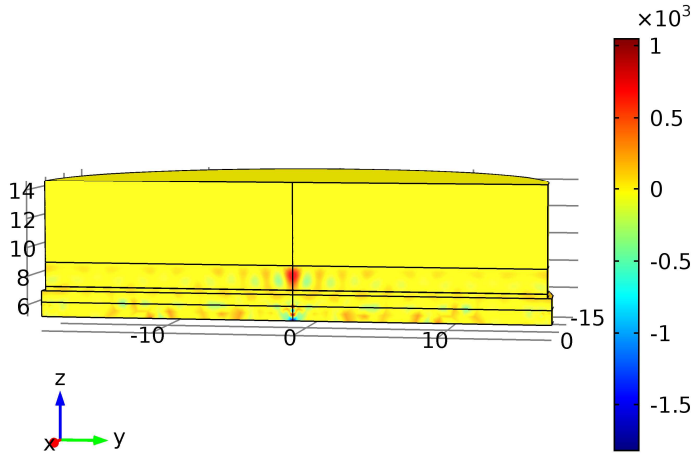

Figure 2-10 presents the result of the temperature after exposure to ultrasound. The maximum temperature was 297.9 K. These results indicates no significant changes in temperature.

**Figure 2-10:** 3D graph of temperature change in the Petri dish.

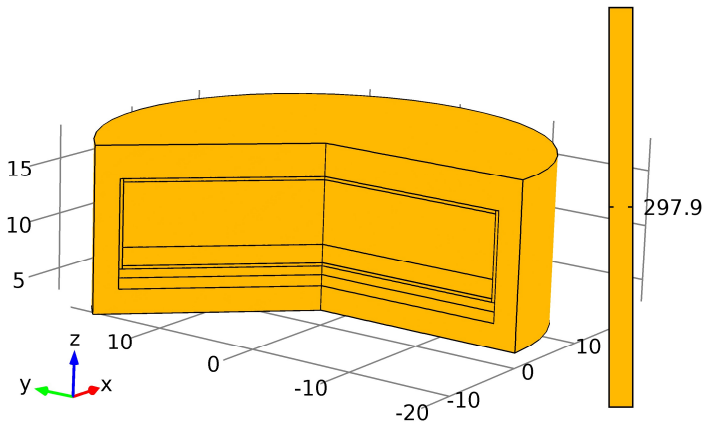


Figure 2-11 shows the internal energy of the cell culture after exposure to ultrasound, i.e. the energy associated with the movement of the particles in each domain. The internal energy cell culture was equivalent to -1.1x10$^3$ J / Kg, indicating little particle movement, and furthermore no significant increase in temperature.

**Figure 2-11:** Graph of cell culture internal energy after exposure to ultrasound

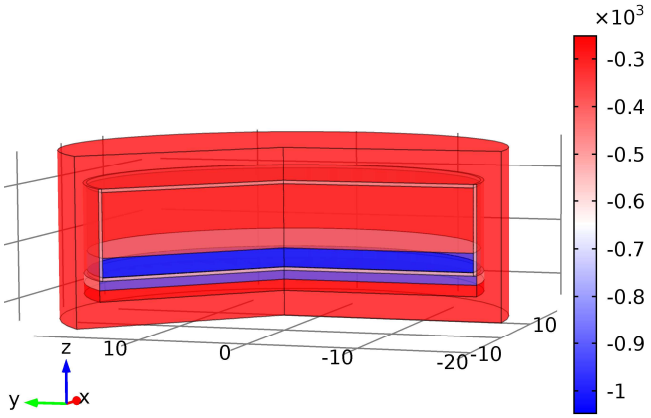

## 2.4 Discussion

This study demonstrates experimentally and computationally that two specific doses of therapeutic ultrasound do not produce thermal effects. In a controlled experiment, cell culture temperature was measured before and after ultrasound treatment. In a computational model, acoustic pressure was determined as a result of applying 1.0 MHz of therapeutic ultrasound, temperature change was evaluated, and cell culture internal energy was calculated upon being exposed to the same acoustic stimulus.

The simulation resulted in a maximum acoustic pressure range of (195 - 308 kPa) for the cell culture and the medium respectively. These values are higher than the pressure exerted by a therapeutic ultrasound of 1.0 MHz (55.7 kPa) on stem cells of dental pulp (Ghorayeb et al., 2013), but lower than the acoustic pressure used in physiotherapy (0.5 MPa) (Cox 2013) and in high frequency ultrasound (1.5 MPa) (Mast et al., 2006). This indicates that ultrasound under the dose presented in this study produces a low-pressure amplitude and does not produce an unstable cavitation effect on the cell culture (Wu & Nyborg 2008).

In a controlled experiment, no significant temperature change was produced in the cell culture domain or other any other domain. This phenomenon is due to the mechanical effect produced by the sound wave on the cells, which responds to the stimulus through mechanotransduction (Miller et al., 2012; Bohari, 2011), (Louw et al., 2013; De Deyne & Kirsch-Volders, 1995).

The internal energy obtained from the cell culture (particle movement) was minimal (-1.1 x103 J / Kg). This measurement indicates non-significant changes in temperature. It is concluded that the specific ultrasound doses applied in this study produce physiological effects due to the mechanical stimulus and not due to thermal effects in cell cultures.

# 3. Effect of the ultrasound stimuli on ligament fibroblast proliferation and extracellular matrix synthesis in vitro

## 3.1 Introduction

Ligament injury is worldwide common pathology, 1 of every 10,000 people suffer an injury per day, and the rehabilitation cost rises to two-billion dollars annually (Rincón Cardozo et al. 2015). Ligaments are a connective tissue made up by cells (fibroblasts) that release and maintain the extracellular matrix, their function is guarantee joint stability, proprioception and loads transfer during body movement (Pedraza Mejías and Martínez Cañadas 2008).

When a ligament is injured due to an overstress, the collagen fibers, blood vessels and nerve fibers are broken (Pedraza Mejías and Martínez Cañadas 2008). This event induces the healing process as follows: “a distinct sequence of cellular events that take place in three consecutive stages: an acute inflammatory phase, a proliferative or regenerative phase, and a tissue remodeling phase” (Hauser et al. 2013).

Therapeutic ultrasound (US) is frequent agent used in physiotherapy to treat the ligament injuries. It works at 1.0 or 3.0 MHz, using low intensities 0.1 to 2.0 W/cm2 (Miller et al., 2012; O’Brien Jr., 2007), and producing energy ranging between 1.0 J/cm$^2$ to 300 J/cm2 (Tole, 2005; Rodríguez, 2008; Baker et al., 2001). Nevertheless, its efficacy is still controversial for clinical use, and scientific evidence to support its impact at the cellular level in ligaments is limited (Louw, Budhiraja, Viljoen, & Subramanian, 2013; De Deyne & Kirsch-Volders, 1995).

Previous findings regarding the effects of ultrasound in other cells as such tendon fibroblasts, gingival, dermic and from connective tissue have shown high collagen synthesis (Ramirez et al. 1997a) (Bohari et al. 2015). Stimulation increased proliferation (Harle et al. 2001b), growth factors (Lai and Pittelkow 2007), focal adhesion proteins (Choi et al. 2011), cellular integrity (Franco de Oliveira et al. 2011) Oliveira et al. 2015), and affected the migration patterns and cellular morphology (Conner-Kerr et al. 2015).

Harle et al., reported that continuous ultrasound at a frequency of 3.0 MHz on periodontal ligament fibroblasts applied at low intensities influenced the expression of collagen type I and fibronectin (Harle et al. 2001b). See more detailed information in Appendix D.

The effect of different doses of pulsed therapeutic ultrasound on ligament fibroblasts obtained from synovial joints in terms of proliferation and extracellular matrix synthesis has not been studied. The aim of this study was to determine whether pulsed ultrasound treatment at 1.0 MHz with two different intensities 1.0 and 2.0 W/cm$^2$ increases (1) collagen type I, type III and fibronectin synthesis using and ELISA assay and (b) cell proliferation through MTS assay by cultured fibroblasts explanted from knee collateral lateral ligament of rat growing as monolayers.

## 3.2 Materials and Methods

To obtain fibroblasts cells that migrated from the ligament onto the surface of the dish, an explant culture technique was used (See 1.2.1). A cell passaging was done in several culture plates to perform both experiments, the enzyme-linked immunosorbent assay (ELISA) extra cellular matrix (ECM) synthesis testing and MTS[4] proliferation assay.

The design for every single experiment consisted in two different stimulated groups treated with ultrasound energy every 24 hours for five days, Group A, received 1.5 W/cm$^2$ and Group B 2.0 W/cm$^2$ doses according to therapeutic range stimulation in cells, and a control Group C was not exposed with ultrasound energy.

To detect collagen type I, type III and fibronectin synthesis in ligament fibroblasts by ultrasound an ELISA testing was performed (Section 3.2.1). To measure cell proliferation by ultrasound a MTS assay was done (Section 3.3.2). Figure 3-1 summarize the designs of both experiments.

[4] MTS: 3-(4,5-Dimethylthiazol-2-yl)-5-(3-carboxymethoxyphenyl)-2-(4-sulfophenyl)-2H-tetrazolium (National Center for Biotechnology Information 2019)

**Figure 3-1:** Experimental design of ELISA testing and MTS assay for this work.

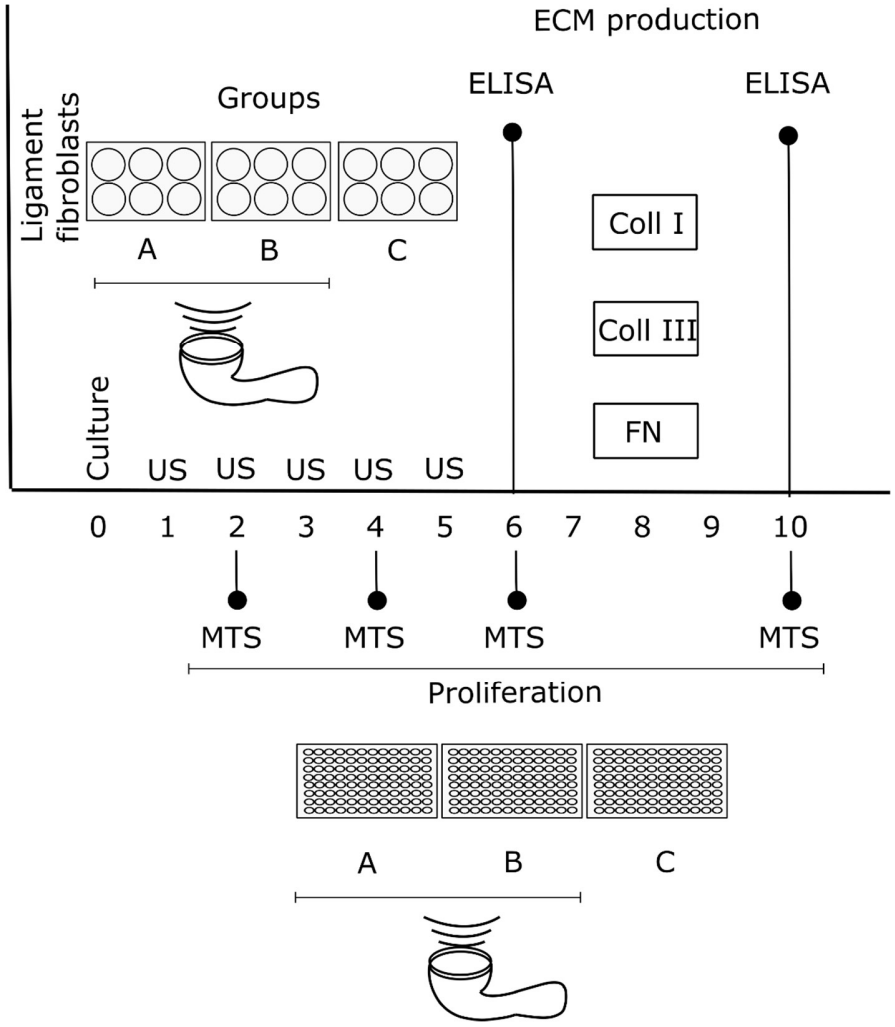


## 3.2.1 ELISA testing

The enzyme linked immunosorbent assay (ELISA) was used to measure the concentration of collagen type I, type III and fibronectin in a conditioned medium (culture supernatant) of ligament fibroblast cells. These cells (1800 cells/well) were cultured in six-well plate per group to obtain 100% confluence on the sixth day (when the treatment had finished).

At this time, the samples of the sixth and tenth culture day (1 mL of culture supernatant for each six-well plate per group) were stored at 4℃ and assayed within 7 days. The medium

was aspired and transferred to the wells of a 96-well ELISA plate following the Rat Collagen Type I (E-EL-R0233), Rat Collagen Type Ⅲ (E-EL-R0235) and Rat Fibronectin (E-EL-R0578) ELISA kit of Elabscience®. Every assay was performed in a different day.

To establish a standard curve for each test, eight diluted concentrations of the typical solution were added in duplicate. For each protein (Collagen type I, Collagen type III, Fibronectin) of every treatment Group A and Group B, we evaluated six samples and three samples for control Group C at sixth day (A6, B6, C6) and tenth day (A10, B10, C10) of culture after the treatment ended (every 24 hours during 5 days).

Besides, we used the standard working solution as a blank control (BL) and culture medium as a negative control (N). A volume of 100 µL/well of the solution standard, samples, blank and negative control was added. The results of each standard and samples were averaged. To determine the optical density (OD) value of each well the microplate was read at 450 nm absorbance.

### 3.2.2 Cell proliferation assay

Ligament fibroblasts (40 cells/well) were cultured in 96-well plate per group to obtain 100% confluence on the sixth day (when the treatment had finished) in a final volume of 200 µL/mL. Wells of every plate were divided into three duplicated groups, each one containing nine wells. The output intensities of ultrasound in the proliferation study were the same used in ELISA testing 1.0 and 2.0 W/cm$^2$ for the treatment Group A and Group B, respectively, and 0.0 W/cm$^2$ for control Group C.

Ligament fibroblasts were exposed to US for 5 days every 24 hours. The MTS assay was adopted to test the cell proliferation on the 1st and 3rd day during stimulation and at 6th and 10th day of culture (after treatment had finished).

The MTS reagent (20 µL) was added directly into cell culture medium following the MTS Cell Proliferation Assay Kit (Colorimetric ab197010) abcam®. Culture plates were incubate for 3 hours at 37 ºC in a 5% CO2 atmosphere.

A microplate reader at 490 nm measured the absorbance. Parallel wells with no cells but the medium contain were set as blank controls. In the control group, the concentration of the MTS assay reagent kept the same as the treated wells. Mean absorbance was calculated from two replicates for each exposure and subtracted values of blank controls.

### 3.2.3 Statistical Analysis

Statistical analysis was completed using BioVinci software version 1.1.3 for Windows 7, developed by BioTuring Inc., San Diego California USA, www.bioturing.com, a software environment for data visualization, analytics, and machine learning for life sciences.

All data was checked for consistency with the Shapiro-Wilk test, Pearson chi-square test, One-sample Kolmogorov-Smirnov test, and Jarque Bera Test. The differences between treatments and controls for each protein, and further discrepancies between all groups were evaluated with the nonparametric multiple comparison Kruskal-Wallis test.

The null and alternative research hypotheses for the nonparametric test were stated as follows: H0: The samples are equal versus H1: The samples are not equal. Differences were at the 5% level of significance.

## 3.3 Results

### 3.3.1 ELISA testing

To evaluate the dependence of extracellular matrix synthesis of rat ligament fibroblasts on the ultrasound stimulation the mean protein optical density (OD) was analyzed. For ligament fibroblasts, the gradual increase in collagen type I, type III and fibronectin expression was upregulated dose dependently after pulsed ultrasound treatment (Figure 3-2).

The optical density (at 450 nm) of type I (0.1 ± 0.04) and type III collagen (0.4 ± 0.2), and fibronectin (0.1 ± 0.02) on ligament fibroblasts increased dose dependently for an intensity of 2.0 W/cm$^2$ at tenth day of culture (five days after treatment), it is showed as B10 in Figure

3-2a. Absorbance of type I (0.04 ± 0.03) and type III collagen (0.07 ± 0.04) for the treatment group measured after stimulation (B6) had the highest value between groups, however, it had lower value than treatment measured five days after stimulation.

Optical density (at 450 nm) of fibronectin (0.03 ± 0.007) for the treatment group measured after stimulation (A6) had the highest value between groups, however, it had lower value than treatment measured five days after stimulation. For all optical density values significant differences were found among the different experiment groups with p-values showed in Figure 3-2b.

**Figure 3-2:** The protein optical density (OD) of cell culture supernatant of rat ligament treated with ultrasound (Groups A and B) every 24 hours for five days and controls (Group C). OD measured at sixth (A6, B6, C6) and tenth (A10, B10, C10) culture days after treatment. (n=6 treatment groups n=3 control groups; *p-values < 0.05). ). a) Rat type I (RCI) and type III collagen (RCIII). b) Rat fibronectin (RF)

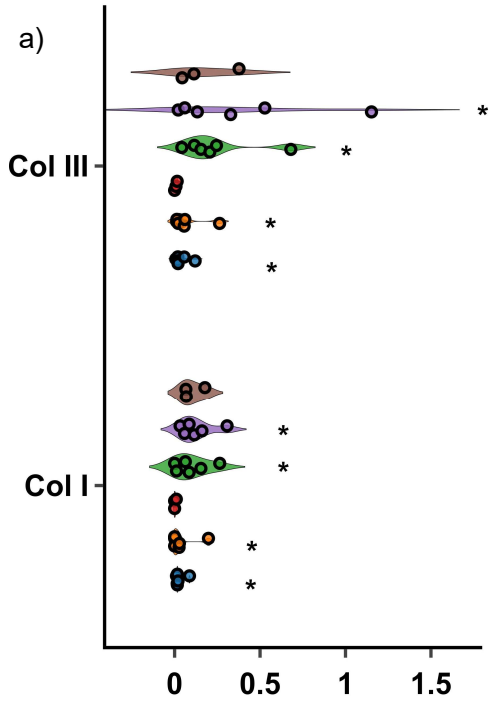

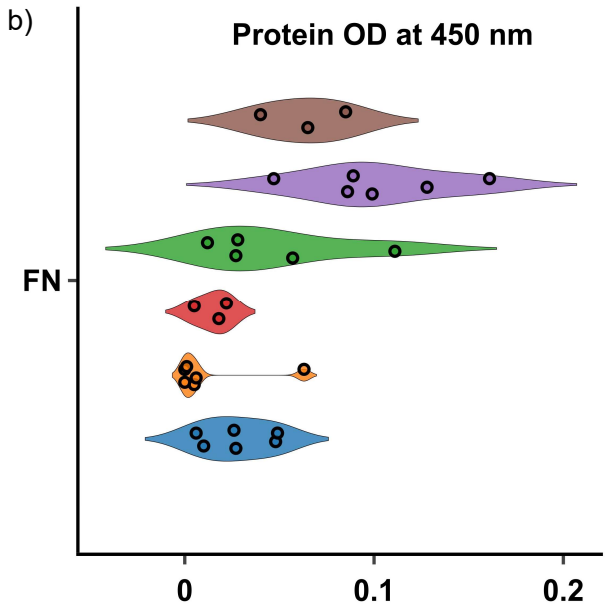


The amount of type I (2.6 ± 1.8 ng/mL) and type III collagen (1.1 ± 0.7 ng/mL), and fibronectin (5.8 ± 1.1 ng/mL) on ligament fibroblasts increased dose dependently for an intensity of 2.0 W/cm$^2$ at tenth day of culture (five days after treatment), it is showed as B10 in Figure 3-3a and Figure 3-3b. Concentration of type I (0.9 ± 0.9 ng/mL) and type III collagen (0.1 ± 0.1 ng/mL) for the treatment group measured after stimulation (B6) had lower protein expression.

Concentration of fibronectin (1.0 ± 0.4 ng/mL) for the treatment group measured after stimulation (A6) had higher protein expression between groups, however, it had lower amount of protein than treatment measured five days after stimulation. For fibronectin significant differences ($p<0.05$) were found among the different experiment groups with p-values showed in Figure 3-3b. We interpreted there is dependence between the level of energy and intensity of the ultrasound and the fibronectin.

When the protein concentration was less than the smallest value of the reference curve, it became cero. For type I and type III collagen expression the values were cero at 1.0 W/cm$^2$ and for Control Group measured after treatment (A6 and C6).

**Figure 3-3**: The protein concentration of cell culture supernatant of rat ligament fibroblasts treated with ultrasound (Groups A and B) every 24 hours for five days and controls (Group C). Concentration measured at sixth (A6, B6, C6) and tenth (A10, B10, C10) days after treatment. (n=6 treatment groups n=3 control groups). a) Rat type I (RCI) and type III collagen (RCIII). b) Rat fibronectin (RF) (*p-value < 0.05). Error bas indicate SEMs

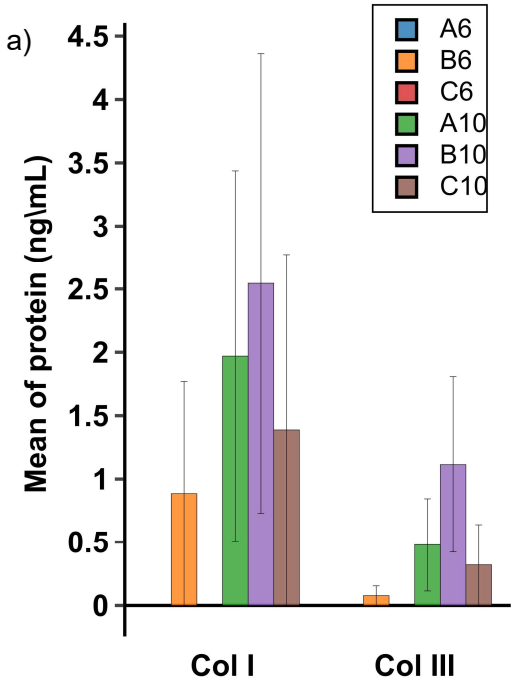

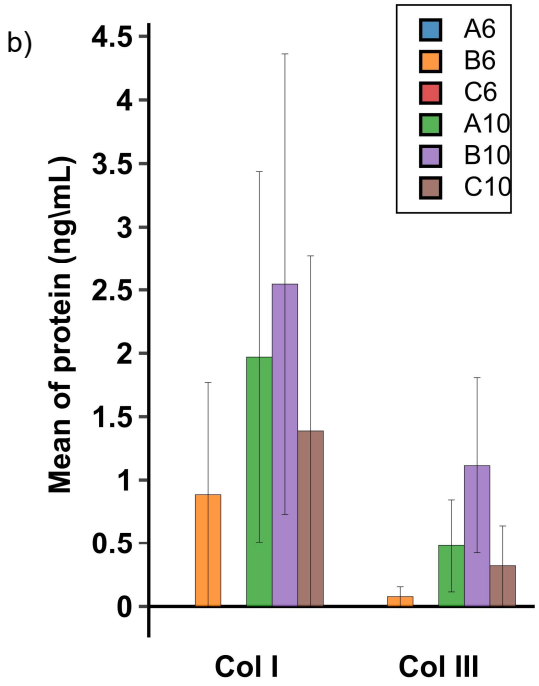


### 3.3.2 MTS assay

On the first day of stimulation (24 h) the cell proliferation assay showed an increase in cell density of 25% for treatment Group A (1.0 W/cm$^2$) compared with the control Group C, but without significance.

On the third day of stimulation (72 h) the cell proliferation assay showed a decrease in cell density of 11% and 9% for treatment groups (A and B), respectively, but without significance (Figure 3-4) .

On the sixth day of culture (144 h) or on the first day after treatment, an increase in cell density of 10% for treatment Group A compared with the control Group C was observed (Figure 3-4) ($P < 0.05$).

On the tenth day of culture (240 h) or on the fifth day after treatment, though a decrease in cell density of 92% and 44% for treatment groups (A and B), respectively, ($P < 0.05$), was found, it may seem strange the decreased cell density for all groups compared with the results obtained on the 6th day of culture.

**Figure 3-4**: Mean of cell density of ligament fibroblasts under different output intensities of ultrasound. Cell proliferation was measured by MTS assay n = 9 duplicated on the first and third day during stimulation and at sixth day and tenth day of culture (after treatment with ultrasound was completed). Data were presented as the mean ± SD. *P<0.05 compared between groups. Error bas indicate SEMs

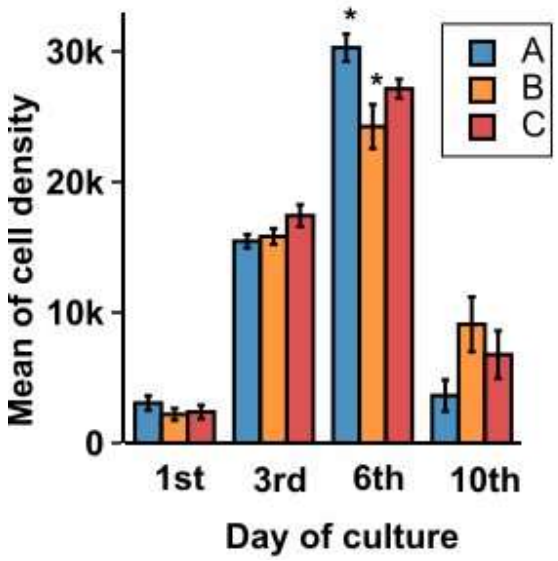


## 3.4 Discussion

In these experiments, we showed the effects of ultrasound on extra cellular matrix synthesis and cell proliferation. Regarding the effect on collagen and fibronectin synthesis, the present experiments demonstrated the dose-dependent stimulatory effect of pulsed ultrasound on collagen type I, type III and fibronectin expression after five days of stimulation at 2 W/cm$^2$.

It has been shown a dose dependence of ultrasound at 1.0 W/cm$^2$ on cell proliferation on the 1st day of stimulation and for the 1st day after treatment. On the same days, the ELISA testing showed non-collagen (type I and III) synthesis. It means low stimulation on cells produced high proliferation and non-collagen protein synthesis.

After treatment the results were similar to those obtained from Donan et al., they found that fibroblasts treated with 1.0 MHz ultrasound showed an increase at 1.0 W/cm$^2$ ($p<0.05$) (Doan et al. 1999)

Collagen type III synthesis was dose dependent of ultrasound at 2.0 W/cm$^2$ after treatment (increased 100%), and it was dependent at 1.0 W/cm$^2$ (increased 33%) and 2.0 W/cm$^2$ (71%) five days after treatment. On the same 1st day after treatment was finished, the proliferation assay showed a decrease (13%) in cell density for treatment Group B (2.0 W/cm$^2$). It means while cells are producing collagen type III they diminished proliferation

These findings are consistent with the observations done by Tsai et al., that concluded that ultrasound stimulates the expression of type I and type III collagen (Tsai et al. 2006).

In contrast to collagen synthesis, fibronectin was dependent of ultrasound at 1.0 W/cm$^2$ after treatment (79%), but decreased (33%) five days after treatment, and increased at 2.0 W/cm$^2$ on the 1$^{st}$ (61%) and 5th day (44%) after stimulation ($p<0.05$). After treatment, proliferation assay showed an increase (10%) in cell density only for treatment Group A (1.0 W/cm$^2$). It means stimulation at low intensity produced high fibronectin protein synthesis and cell proliferation as well

Similar results were obtained by Harle et al., which found on a human osteoblast-like cell line that fibronectin was up-regulated at low intensities of ultrasound, however different results were found on human periodontal ligament cells (Harle et al. 2001a). These differences may be explained by different doses of stimulation and a diverse cell culture type.

These findings demonstrate that therapeutic ultrasound may influence on ligament repair and healing processes through increasing the synthesis of proteins of the extracellular matrix, and suggest that the parameters of ultrasound could be controlled to stimulate cells to improve either stage of healing, early phase or regenerative (cell proliferation), or late phase called remodeling (protein extracellular matrix production).

# 4. Effect of the ultrasound stimuli on ligament fibroblast migration

## 4.1 Introduction

Ligaments are dense connective tissue that stabilize and provide tensile strength to an articulating joint (Foote 2017; Larson 2017). They are composed of a cellular component called fibroblasts that maintain and produce extracellular matrix (Larson 2017; Trepat et al. 2012). When tissue has been injured, fibroblasts are activated to migrate, proliferate, and synthesize extracellular matrix into the wounded area during the ligament healing process (Cottrell et al. 2016).

Cell migration is a fundamental process by which cells move from one location to another. In ligament healing, fibroblasts move into the site of injury to produce the new extracellular matrix (Dutton 2011; Springer Nature 2019; Vicente-Manzanares 2005). Its motility is featured by the leading edge that indicates the direction of displacement and is driven by actin cytoskeleton polymerization (Vicente-Manzanares 2005).

Therapeutic ultrasound stimulates several processes within the fibroblast as proliferation (De Deyne and Kirsch-Volders 1995; Leng et al. 2018) and collagen synthesis (Carrer et al. 2015; Ramirez et al. 1997b) through the activation of calcium influx and altering plasma membrane's permeability (Dinno et al. 1989). Roper et al, also found an intracellular mediator of fibroblast migration into the wounded area called Rac1 due to ultrasound treatment (Roper et al. 2015).

A typical wound closure assay is widely used in the scientific community. It examines the ability of a particular cell line to migrate and subsequently close a wound made in confluent plate of cells (Justus et al. 2014). To simulate the wounded area a "scratch" is made on a cell monolayer. Then, images are captured and compare the beginning and at specific

intervals during cell motility to close the scratch (Bise et al. 2011; Justus et al. 2014; Liang et al. 2007; Trepat et al. 2012).

Although ultrasound has be shown to affect the migration of different types of cells in vitro with several doses (Atherton et al. 2017; Leng et al. 2018; Mohammed et al. 2016; Zhou et al. 2018), the studies on ligament fibroblast (from articulating joints) migration are limited. The present study attempted to assess the effect of therapeutic ultrasound on ligament cell migration using a scratch assay.

## 4.2 Materials and Methods

To obtain ligament fibroblasts an explant culture technique was used (See section 1.2.1). When monolayer cultures were confluent they were detached using 0.025% trypsin (Gibco-Vitrogen Corporation) for five minutes and subcultured on several twelve-well plates for migration testing. They were maintained in 1 mL of supplemented (10% Fetal Bovine Serum and 1% antibiotics) culture medium DMEM/F12 at 37 ºC in a 5% CO2 atmosphere. The medium was changed every 48 hours.

A total of 500 cells were monolayer cultured in nine wells of twelve-well plates per group (see Figure **4-1**) to obtain 100% confluence on the sixth day (when treatment has finished). Two different treated groups were stimulated with ultrasound intensity every 24 hours for five days (See section 1.2.2), Group A, received 1.0 W/cm$^2$ and Group B 2.0 W/cm$^2$ according to the therapeutic range stimulation in cells, and a control Group C was processed in the same way as the stimulated group, but without exposure to ultrasound energy.

**Figure 4-1**. Method design of the wound scratch assay to measure cell migration for treated groups with ultrasound Group A (1.0 W/cm$^2$) and Group B (2.0 W/cm$^2$) and control Group C.

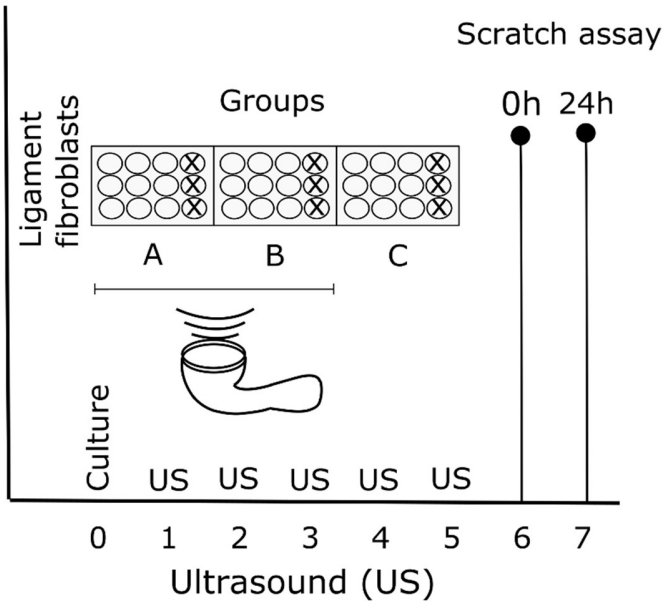


To measure ligament fibroblasts migration we used the *in vitro* scratch assay proposed by Liang et al., (Liang et al. 2007). 24 hours after ultrasound treatment was completed, we changed the culture medium without fetal bovine serum to control cell division. Then, we created a “scratch” in a cell monolayer using a 10-μL tip, capturing the images at the beginning and within 24 hours when fibroblasts migration closed the scratch using a Cytation 3 Cell Imager Multi-Mode Reader (Biotek) and the software Gen 5.2.0.7 (Biotek)(See Figure 4-2).

Single blinded for migration assay was carried out. Six measurements were taken with respect to a vertical line that defined the reference axis on every captured image along each cell distance (1 pixel equal to 1 μm). We measured how far along every cell was using the software ImageJ version 1.50i 3 for Windows 7, developed by Wayne Rasband, National Institute of Health USA, http://imagej.nih.gov/ij. In total 82 (we lost 20 images due low image quality), 102, and 107 images were taken per group.

An example of the *in vitro* scratch assay is shown in Figure 4-2a to Figure 4-2d, as well as the six marked points and their length, respectively for every group. The vertical lines define the reference axis to measure the cell length and horizontal lines define the length from the cell to the reference axis. In this case, we established the difference between the two

measurements, 24 hours at the beginning and within 24 hours of migration to each marked point. The mean of these differences was used to determine the length of cell migration for each group.

**Figure 4-2**. Analysis of cell migration by in vitro wound scratch assay. Images were acquired at 0 h and 24 h for treatment Group A (a) and (b), Group B (c) and (d), and control Group C (e) and (f), respectively.

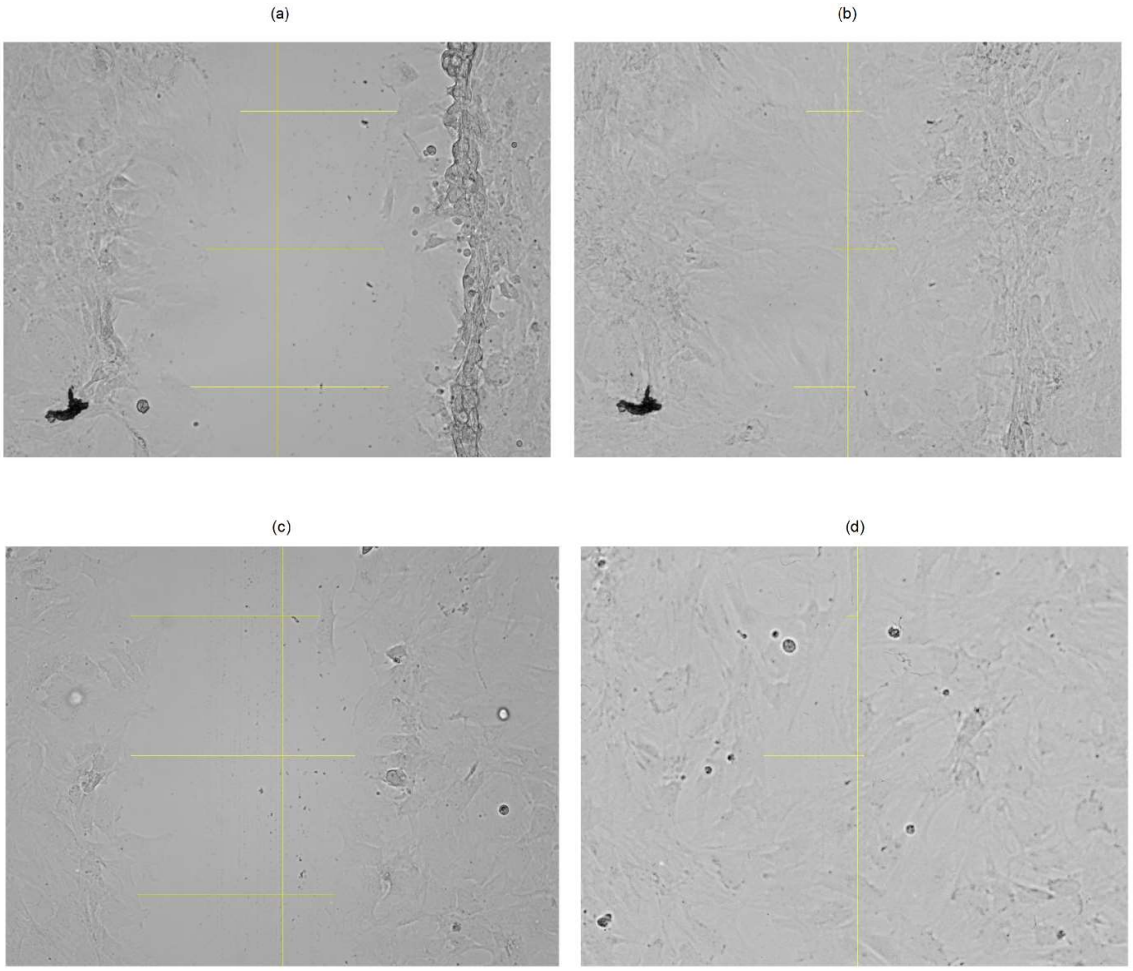

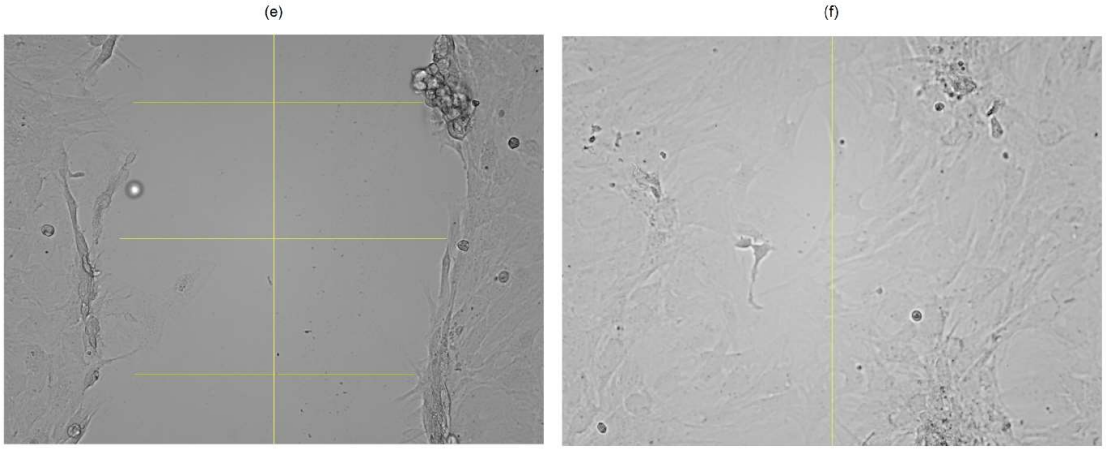


We analyzed 494 measurements for treatment Group A, 613 for treatment Group B and 641 for the Control Group. Statistical analysis was completed using BioVinci software version 1.1.3 for Windows 7, developed by BioTuring Inc., San Diego California USA, www.bioturing.com, a software environment for data visualization, analysis, and machine learning for life sciences.

All data was checked for normality with the Shapiro-Wilk test, Pearson chi-square test, One-sample Kolmogorov-Smirnov test, and Jarque Bera test, however the data was non-normally distributed. The differences between treatments and control groups were evaluated with the nonparametric multiple comparison Kruskal-Wallis test.

The null and alternative research hypotheses for the nonparametric test were stated as follows: H0: The samples are equal versus H1: The samples are not equal. Differences were at the 5% level of significance.

## 4.3 Results

Ultrasound stimulation has shown to increase the mean migration length (μm) over a 24 h period of ligament fibroblasts when cells are stimulated at 1.0 W/cm$^2$ (Treatment Group A). On the contrary, it was interesting to see that ultrasound stimulation at 2.0 W/cm$^2$ (Treatment Group B) decreased the mean migration length (μm).

As can be seen by Figure **4-3**, when comparing the treatment Group A with control Group C, there was an increase in mean migration distance of approximately 11 µm (4%). In contrast, when comparing the treatment Group B with control Group C, there was a decrease in mean migration distance of approximately 29 µm (11%).

**Figure 4-3:** Mean of migration length (µm) over 24 h period (after treatment with ultrasound was completed) for ligament fibroblasts treated at 1.0 W/cm$^2$ (Group A), at 2 W/cm$^2$ and non-treated (Group C).

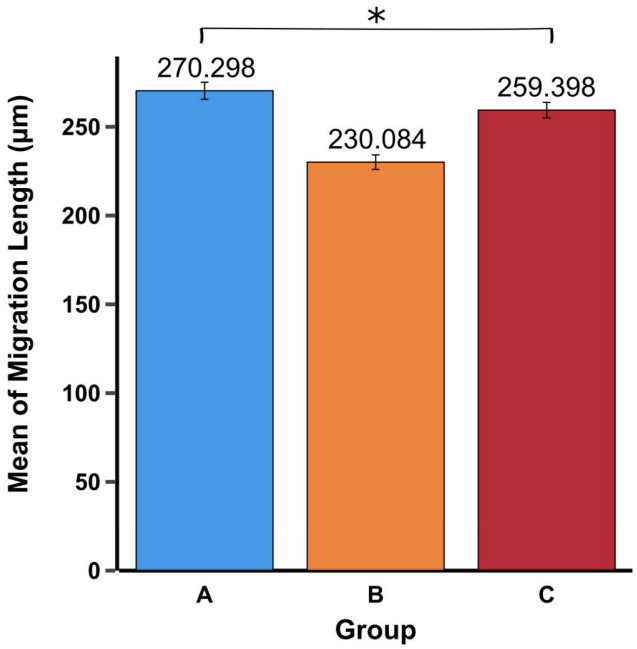


Figure **4-4** showed boxplots which displayed differences between populations without making any assumptions of the underlying statistical distribution: they are non-parametric. As statistical analysis showed p-value was less than the significance level of 0.05, we interpreted that there was dependence between the energy level and ultrasound intensity and the cell migration.

**Figure 4-4:** Box plot of mean of migration length (µm) over 24 h period (after treatment with ultrasound was completed) for ligament fibroblasts treated at 1.0 W/cm$^2$ (Group A), at 2.0 W/cm$^2$ and non-treated (Group C).

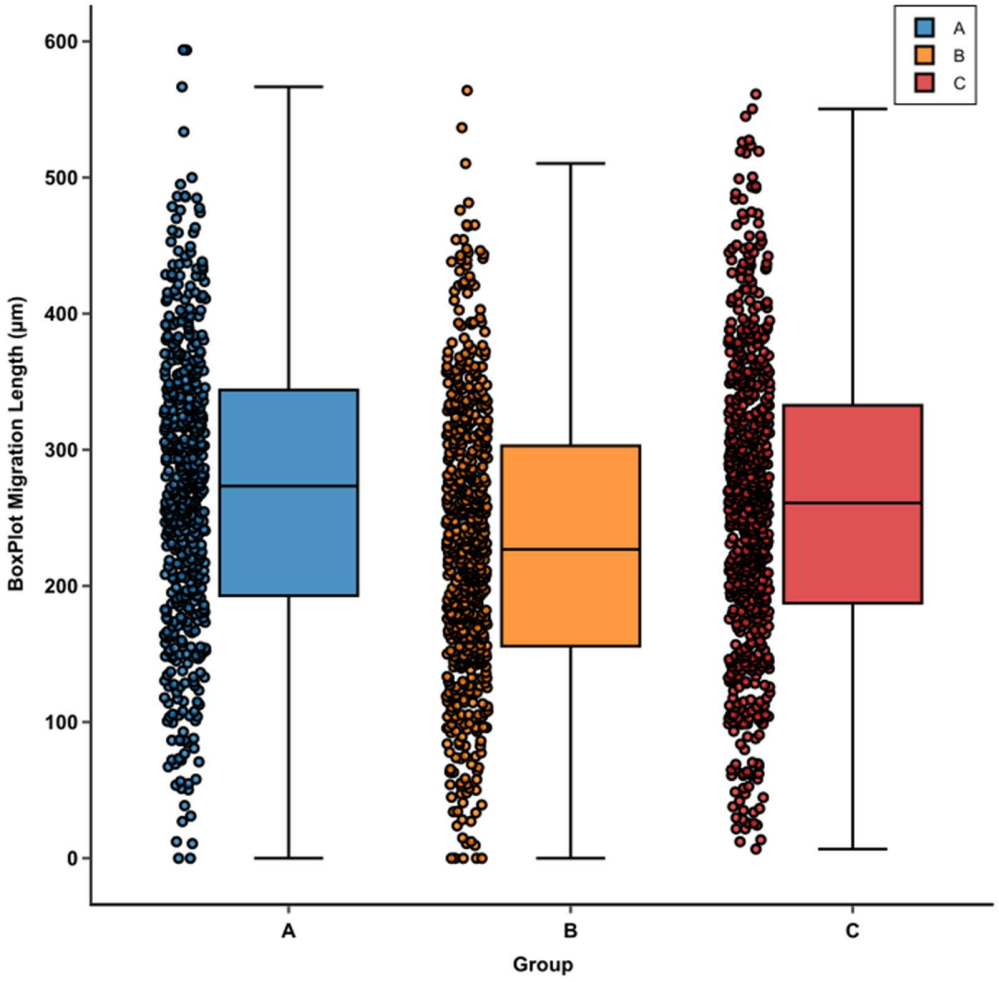


## 4.4 Discussion

In this study we evaluated ligament fibroblast migration under two different doses of ultrasound at 1.0 MHz with intensity doses of 1.0 W/cm$^2$ and 2.0 W/cm$^2$ pulsed with a duty cycle of 50%. We found that migration increased 4% and decreased 11% due to the stimulation at a lower and higher intensity, respectively. We used the statistical mean length (µm) to compare the migration and demonstrated significant differences between the different experiment groups ($p < 0.05$).

It has been shown that cells proliferate and migrate into the wound area to produce the new extracellular matrix (Cottrell et al. 2016). Hence, adequate ligament healing requires fibroblasts proliferation, migration, as well as suitable extracellular matrix synthesis (type I and III collagen and fibronectin expression). These findings provide potential mechanisms for using therapeutic ultrasound to treat ligament injuries.

Therapeutic ultrasound uses a typical frequency of 1.0 MHz and intensity in the range of 0.5-2.0 W/cm$^2$. Its energy can be delivered in a continuous or pulsed manner, with duty factor ranging from 10-50% Pulsed mode produces non-thermal effects (Draper and Prentice 2011; Eggers and Onks 2019). The ultrasound doses used in this study are consistent with what is used clinically in rehabilitation.

We noted our experimental cell migration results were somewhat consistent with similar work reported in the literature. For example, Tsai et al., demonstrated that dose-dependent ultrasound at 1.0 MHz with 20% duty cycle at 0.1 W/cm$^2$, 0.5 W/cm$^2$ and 1 W/cm$^2$ enhanced tendon cells migration and proliferation at 31%, 35% and 52%, respectively (Tsai et al. 2008).

For osteoblast migration cultures that were exposed to continuous 45 kHz ultrasound at 25 mW/cm$^2$ or pulsed 1.0 MHz at 250 mW/cm$^2$ for 30 min followed by 2 days culture. Ultrasound significantly enhanced cell migration (wound closure) by 40% (Man et al. 2012).

Mohammed et al., found that fibroblast cell migration was increased by 10% using mechanical stimulation at 100 Hz of acoustic vibration on a single cell for 5 minutes. However, cell migration was decreased by 48% at 1600 Hz on fibroblast lung cells (Mohammed et al. 2016).

Contradictory results were observed in normal human urothelial cell monolayers migration that were exposed to clinical doses of low pulsed ultrasound at 1.5 MHz for 20 min (daily) pulsed at 1 kHz a 20% duty cycle with intensity of 30 mW/cm$^2$. Cultures showed no change in migration or cell growth (Hill et al. 2005).

Aterthon et al., demonstrated that low intensity pulsed ultrasound at 1.2 MHz with intensity of 30 mW/cm$^2$ for 20 min. improves migration speed of osteoblasts (MC3T3) at 30% through integrin-mediated cell-matrix adhesion, inducing Rac 1 (small G protein) activation that produces actin cytoskeleton reorganization in order to migrate (Atherton et al. 2017).

Leng et al., showed that low intensity pulsed ultrasound at 0.5 MHz for 1 min with spatial temporal average sound pressure of 0.3 MPa promoted a relative migration at 150% and proliferation at 80% for keratinocytes cells by activating the PI3K/AKT and JNK pathways (Leng et al. 2018) that transduce the extracellular signals like ultrasound stimuli into cell migration, through a regulation of microtubule stability (Onishi et al. 2007).

The effect of therapeutic ultrasound on cell migration depends on several cell types and ultrasound doses. Through literature analysis, we conclude that pulsed ultrasound may stimulate cell migration through cytoskeleton protein rearrangement and fibronectin synthesis. Cells need to migrate to the wound area to produce new extracellular matrix giving the tissue strength and structural integrity.

In this study, we showed therapeutic ultrasound at 1.0 MHz with intensity of 1 $W/cm^2$ increases cell migration on ligament fibroblast and it may improve the ligament healing through cytoskeleton reorganization and increased fibronectin synthesis that activates mechanotransduction signal pathways.

# 5. Conclusions and recommendations

In this work, the effects of several doses of therapeutic ultrasound on the mechanical and biological behavior of ligament fibroblasts was evaluated. Considering that ligament-healing process depends on cell functionality and dose of the stimulus, we measured fibroblast elastic modulus, viability, proliferation, extracellular matrix synthesis and migration. It was demonstrated that mechanical and biological properties of fibroblasts are dependent of therapeutic ultrasound and it can improve the ligament healing process.

Bearing in mind that the mechanical behavior is related with cell functionality and motility, we measured cell elastic modulus through AFM testing, that significantly decreased 22% and 31% owing to the application of pulsed therapeutic ultrasound at 1.0 MHz for treatment Group A (1.0 W/cm$^2$) and Group B (2.0 W/cm$^2$), respectively. While cell elastic modulus reflects indentation resistance of the cell cytoskeleton with AFM tip, the data suggests that cell cytoskeleton structure is significantly deformable upon the applied energy density.

To understand why the elastic modulus of the cell cytoskeleton decreased, first, we asked if ultrasound produced a resonance effect that could induce alterations or cellular death. Through computational modelling we found that harmonics were in the order of kilohertz and higher than 17.0 MHz, and the cell cytoskeleton frequency of control Group C was found to be 20% greater than cytoskeleton of stimulated cells (50th frequency of vibration).

The second objective focused on the detection of damaged or dying cells, by the assessment of fibroblast viability through fluorochrome staining (annexin and propidium iodide) for flow cytometry assay. We showed that cell viability compared to control group diminished in 1% and 10% for treatment Group A (1.0 W/cm$^2$) and Group B (2.0 W/cm$^2$), respectively. We can infer that therapeutic ultrasound at 1.0 MHz produces a low chance of causing resonant effect, guaranteeing that cells can still be viable.

As results indicated that therapeutic ultrasound at 1.0 MHz for both intensities did not produce cell damage, we hypothesized cells rearrange their cytoskeleton in order to 1) migrate into a wounded area or 2) resist deformation during their metabolic activity. This explains why cells decreased their elastic modulus. Consequently, we evaluated cell

proliferation, extracellular matrix synthesis (Type I and III collagen and fibronectin), and migration.

To assess cell proliferation, we measured cell enzyme activity through colorimetric assay (MTS), finding that cell proliferation was increased 10% for treatment Group A, and decreased 13% for treatment Group B; results also demonstrated significant differences among groups ($p< 0.05$). This may be understood by the fact that cell division may be increased due to a low intensity ultrasound, and decreased by higher one.

Collagen synthesis is important to provide resistance to the new tissue. Type I collagen was increased 100% for treatment Group B, and no synthesis was detected for treatment Group A and control Group C. Fibronectin was increased 79% and 61% for treatment Group A and B, after treatment ($p<0.05$).

Considering that the early stage of healing continues several weeks after injury, proteins of the extracellular matrix synthesis were also measured during five days after treatment. Type I and type III collagen was increased 45% and 71% for high intensity, and increased 30% and 33% for low intensity. Fibronectin was decreased 33% for treatment Group A, and increased 44% for treatment Group B ($p<0.05$).

Summarizing, levels of collagen were raised for stimulated groups five days after treatment, and only for stimulated Group B after treatment. Levels of fibronectin were increased in both treatment groups, and more significantly increasing for treatment Group B, five days after treatment. It means a dose-dependent stimulatory effect of pulsed ultrasound on type I and type III collagen, and fibronectin expression according the day after treatment.

Finally, migration was evaluated by measuring the displacement of cells into a wounded area through scratch assay. We have shown that migration (mean length μm) increased 4% and decreased 11% owing to the stimulation at lower and higher intensity, respectively, and demonstrated significant differences among the different experiment groups ($p< 0.05$). It means cell motility is significantly dependent upon the lower dose of ultrasound.

Our findings suggested that specific doses of ultrasound may improve either stage of healing, early (regenerative) or late phase (remodeling). While collagen synthesis was high, the fibronectin synthesis was low, and cell elastic modulus, proliferation and migration was

decreased (treatment Group B). While collagen production and cell elastic modulus was low, the fibronectin synthesis, cell proliferation and migration was high (treatment Group A). In summary, this work argued that pulsed therapeutic ultrasound might be used to stimulate cells to improve the ligament healing process.

There are several limitations to this study including 1) it was used a pyramidal tip in AFM testing. Though we used the asymptotical correction model for rigid cone indenting to nullify the dependence of the depth indentation, spherical tip could be also tested to measure the variability of cell elastic modulus for treatment and control groups.

2) The geometry simulated to calculate harmonics has been simplified to represent cell cytoskeleton, since it is the structure that resist the deformation against external mechanical stimuli. However, we suggest to include the cytosol and nucleus in the computational model to evaluate the changes of harmonics in whole cell.

3) To improve comprehension of the mechanisms underlying responses of cells to ultrasound, future research on molecular markers is suggested. For example, evaluate the dynamic of actin polymerization and disassembly due to ultrasound by detecting molecular targets that can be related with cell migration.

Summary of findings is showed in Table 5-1.

Table 5-1. Summary of findings

| Pulsed ultrasound at 1.0 MHz | Treatment Group A (1.0 W/cm$^2$) | Treatment Group B (2.0 W/cm$^2$) | Comments | |
|---|---|---|---|---|
| Variable | Percentage difference | | | |
| Elastic modulus | ↓22% | ↓31% | Percentage difference was calculated comparing to control Group C | |
| Harmonic vibration | ↓20% | ↓20% | Percentage difference was calculated comparing to control Group C with respect to 50th frequency of vibration | |
| Viability | ↓1% | ↓10% | Percentage difference was calculated comparing to control Group C | |
| Level of protein synthesis | | | | |
| Protein | 1st day after treatment with ultrasound was completed (6th day of culture) | | 5th day after treatment with ultrasound was completed (10th day of culture) | |
| | Treatment Group A6 (1.0 W/cm$^2$) | Treatment Group B6 (2.0 W/cm$^2$) | Treatment Group A10 (1.0 W/cm$^2$) | Treatment Group B10 (2.0 W/cm$^2$) |
| Type I collagen | ↑ Very low | ↑↑ Low | ↑↑↑ Moderate | ↑↑↑↑ High |
| Type III collagen | ↑ Very low | ↑↑ Low | ↑↑↑ Moderate | ↑↑↑↑ High |
| Fibronectin | ↑↑↑ Moderate | ↑↑ Low | ↑↑↑ Moderate | ↑↑↑↑ High |
| Proliferation | ↑10% | ↓13% | Percentage difference was calculated comparing to control Group C | |
| Migration | ↑4% | ↓11% | Percentage difference was calculated comparing to control Group C | |

# A. Appendix: Python script to create the cytoskeleton

Python script to create the cytoskeleton (octahedron tensegrity) structure in Abaqus CAE for the A, B, and C configuration.

```
#####################CELLID27#Group_A#################
#Octahedron tensegrity for Group A
#
#Contact diameter (22.4 um) - Reference(Mcgarry & Prendergast, 2004)
#50% - Contact radius (11.2 um)
#25% - Half contact radius (5.6 um)
#75% - 3 times half Contact radius (16.8 um)
#
#Cell Height taken from AFM results(4.6 µm)
#50% - Half =2.3
#25% Half of half =1.1
#75% 3 times Half/half Cell Height = 3.4#
#
p = mdb.models['CELL-ID28-a'].parts['Part-1']
session.viewports['Viewport: 1'].setValues(displayedObject=p)
p.DatumPointByCoordinate(coords=(22.4,2.3,5.6))
p.DatumPointByCoordinate(coords=(0.0,2.3,5.6))
p.DatumPointByCoordinate(coords=(22.4,2.3,16.8))
p.DatumPointByCoordinate(coords=(0.0,2.3,16.8))
p.DatumPointByCoordinate(coords=(16.8,4.6,11.2))
p.DatumPointByCoordinate(coords=(16.8,0.0,11.2))
```

```
p.DatumPointByCoordinate(coords=(5.6,4.6,11.2))
p.DatumPointByCoordinate(coords=(5.6,0.0,11.2))
p.DatumPointByCoordinate(coords=(11.2,3.4,0.0))
p.DatumPointByCoordinate(coords=(11.2,3.4,22.4))
p.DatumPointByCoordinate(coords=(11.2,1.1,0.0))
p.DatumPointByCoordinate(coords=(11.2,1.1,22.4))
d = p.datums
p.WirePolyLine(points=((d[2], d[3]),(d[4], d[5]),(d[6], d[7]),(d[8], d[9]),(d[10], d[11]),(d[12], d[13]),(d[3], d[12]),(d[5], d[13]),(d[4], d[13]),(d[2], d[12]),(d[8], d[10]),(d[6], d[10]),(d[11], d[5]),(d[10], d[3]),(d[10], d[2]), (d[11], d[4]),(d[9], d[12]),(d[3], d[9]),(d[5], d[9]),(d[7], d[4]),(d[7], d[2]),(d[8], d[3]), (d[8], d[5]),(d[6], d[2]),(d[6], d[4]),(d[7], d[13]), (d[8], d[11]),(d[6], d[11]),(d[9], d[13]),(d[12], d[7]) ), mergeWire=OFF, meshable=ON)
p = mdb.models['CELL-ID28-a'].parts['Part-1']
#End


# # # # # # # # # # # # # # # # # CELLID27# Group_B## # # # # # # # # # # # # # # #
 #Octahedron tensegrity for Group B
#
#Contact diameter (22.4 um) - Reference(Mcgarry & Prendergast, 2004)
#50% - Contact radius (11.2 um)
#25% - Half contact radius (5.6 um)
#75% - 3 times half Contact radius (16.8 um)
#
#Cell Height taken from AFM results(3.1 μm)
#50% - Half =1.6
#25% Half of half =0.8
#75% 3 times Half/half Cell Height = 2.3
#
p = mdb.models['CELL-ID28-b'].parts['Part-1']
session.viewports['Viewport: 1'].setValues(displayedObject=p)
p.DatumPointByCoordinate(coords=(22.4,1.6,5.6))
p.DatumPointByCoordinate(coords=(0.0,1.6,5.6))
```

```
p.DatumPointByCoordinate(coords=(22.4,1.6,16.8))
p.DatumPointByCoordinate(coords=(0.0,1.6,16.8))
p.DatumPointByCoordinate(coords=(16.8,3.1,11.2))
p.DatumPointByCoordinate(coords=(16.8,0.0,11.2))
p.DatumPointByCoordinate(coords=(5.6,3.1,11.2))
p.DatumPointByCoordinate(coords=(5.6,0.0,11.2))
p.DatumPointByCoordinate(coords=(11.2,2.3,0.0))
p.DatumPointByCoordinate(coords=(11.2,2.3,22.4))
p.DatumPointByCoordinate(coords=(11.2,0.8,0.0))
p.DatumPointByCoordinate(coords=(11.2,0.8,22.4))
d = p.datums
p.WirePolyLine(points=((d[2], d[3]),(d[4], d[5]),(d[6], d[7]),(d[8], d[9]),(d[10], d[11]),(d[12], d[13]),(d[3], d[12]),(d[5], d[13]),(d[4], d[13]),(d[2], d[12]),(d[8], d[10]),(d[6], d[10]),(d[11], d[5]),(d[10], d[3]),(d[10], d[2]), (d[11], d[4]),(d[9], d[12]),(d[3], d[9]),(d[5], d[9]),(d[7], d[4]),(d[7], d[2]),(d[8], d[3]), (d[8], d[5]),(d[6], d[2]),(d[6], d[4]),(d[7], d[13]), (d[8], d[11]),(d[6], d[11]),(d[9], d[13]),(d[12], d[7]) ), mergeWire=OFF, meshable=ON)
p = mdb.models['CELL-ID28-b'].parts['Part-1']
#End

################## CELLID27# Group_C################
#Octahedron tensegrity for Group C
#
#Contact diameter (22.4 um) - Reference(Mcgarry & Prendergast, 2004)
#50% - Contact radius (11.2 um)
#25% - Half contact radius (5.6 um)
#75% - 3 times half Contact radius (16.8 um)
#
#Cell Height taken from AFM results(2.7 µm)
#50% - Half =1.4
#25% Half of half =0.7
#75% 3 times Half/half Cell Height = 2.0
#
p = mdb.models['CELL-ID28-c'].parts['Part-1']
session.viewports['Viewport: 1'].setValues(displayedObject=p)
```

```
p.DatumPointByCoordinate(coords=(22.4,1.4,5.6))
p.DatumPointByCoordinate(coords=(0.0,1.4,5.6))
p.DatumPointByCoordinate(coords=(22.4,1.4,16.8))
p.DatumPointByCoordinate(coords=(0.0,1.4,16.8))
p.DatumPointByCoordinate(coords=(16.8,2.7,11.2))
p.DatumPointByCoordinate(coords=(16.8,0.0,11.2))
p.DatumPointByCoordinate(coords=(5.6,2.7,11.2))
p.DatumPointByCoordinate(coords=(5.6,0.0,11.2))
p.DatumPointByCoordinate(coords=(11.2,2.0,0.0))
p.DatumPointByCoordinate(coords=(11.2,2.0,22.4))
p.DatumPointByCoordinate(coords=(11.2,0.7,0.0))
p.DatumPointByCoordinate(coords=(11.2,0.7,22.4))
d = p.datums
p.WirePolyLine(points=((d[2], d[3]),(d[4], d[5]),(d[6], d[7]),(d[8], d[9]),(d[10], d[11]),(d[12],
d[13]),(d[3], d[12]),(d[5], d[13]),(d[4], d[13]),(d[2], d[12]),(d[8], d[10]),(d[6], d[10]),(d[11],
d[5]),(d[10], d[3]),(d[10], d[2]), (d[11], d[4]),(d[9], d[12]),(d[3], d[9]),(d[5], d[9]),(d[7],
d[4]),(d[7], d[2]),(d[8], d[3]), (d[8], d[5]),(d[6], d[2]),(d[6], d[4]),(d[7], d[13]), (d[8], d[11]),(d[6],
d[11]),(d[9], d[13]),(d[12], d[7]) ), mergeWire=OFF, meshable=ON)
p = mdb.models['CELL-ID28-c'].parts['Part-1']
#End
```

# B. Appendix: Statistical Analysis including the results of the multicomparison tests for the Cell Death assay.

Statistical analysis was completed using BioVinci software version 1.1.3 for Windows 7, developed by BioTuring Inc., San Diego California USA, www.bioturing.com., a software environment for data visualization, analytics, and machine learning for life sciences.
For each region from the data generated by flow cytometry (Necrotic cells (Q1), Late apoptosis (Q2), Viable cells (Q3), Early apoptosis (Q4)) for treatment Groups (A and B) and control Group (C), a sample size of 2, was analyzed. The samples corresponded to a ten thousand test runs. A nonparametric univariate Kruskal-Wallis test was therefore used. The null and two-sided research hypotheses for the nonparametric test were stated as follows: H0: The population medians for these groups are all equal versus H1: the population means for these groups are all not equal. Differences were at the 5% level of significance.
Results

In these results, the sample estimated of the means for the three groups (A, B, C) for each region from the data generated by flow cytometry (Necrotic cells (Q1), Late apoptosis (Q2), Viable cells (Q3), Early apoptosis (Q4)). The null hypothesis states that the population means for these groups are all equal. For Q1, Q2, Q3 and Q4 no significant differences were found among the different experiment groups with p-value = 0.95. Groups A, B and C received p-value(Q1) = 0.6514, p-value(Q2) = 0.5647, p-value(Q3) = 0.1801 and p-value(Q4) = 0.1801. Because all p-values are greater than the significance level of 0.05, we don't reject the null hypothesis and conclude that the means are all equal. We

interpreted there is no dependence between the level of energy and intensity of the ultrasound and the cell death.

The results obtained in the statistical software are shown below:

**********Kruskal-Wallis rank sum test for the three groups (A, B, C) **********

**********Using BioVinCi version 1.1.3 for Windows 7**********

**********Results in R: Q1 **********

Kruskal-Wallis chi-squared = 0.85714, df = 2, p-value = 0.6514

**********Results in R: Q2**********

Kruskal-Wallis chi-squared = 1.1429, df = 2, p-value = 0.5647

**********Results in R: Q3 **********

Kruskal-Wallis chi-squared = 3.4286, df = 2, p-value = 0.1801

**********Results in R: Q4 **********

Kruskal-Wallis chi-squared = 3.4286, df = 2, p-value = 0.1801

**********End Kruskal-Wallis analysis**********

Here the treatment and control groups are shown below:

A: Treatment group (1.0 W/cm2)

B: Treatment group (2.0 W/cm2)

C: Control group (0 W/cm2).

# C. Appendix: Statistical Analysis including the results of the multicomparison tests for the Elastic Modulus.

Statistical analysis was completed using BioVinci software version 1.1.3 for Windows 7, developed by BioTuring Inc., San Diego California USA, www.bioturing.com., a software environment for data visualization, analytics, and machine learning for life sciences.
Analysis results from Pearson chi-square normality test, One-sample Kolmogorov-Smirnov test, Jarque Bera Test an Shapiro-Wilk normality test, demonstrated that the distributions of elastic modulus for treatment Groups (A and B) and control Group (C) were not normal. From each group, a sample size of 863, 866, and 338, respectively, was analyzed.
A nonparametric multiple comparison using a Kruskal-Wallis test was therefore used to compare groups A, B and C. The null and two-sided research hypotheses for the nonparametric test were stated as follows: H0: The two samples are equal versus H1: The two samples are not equal. Differences were at the 5% level of significance.
Results

Significant differences were found among the different experiment groups using the Kruskal-Wallis non-parametric test with p-value 6.3e-22. Hence $p < 0.05$ for all comparisons, we reject the null hypothesis that the groups are equal with respect to the elastic modulus.
The results obtained in the statistical software are shown below:
**********Results Kruskall test using BioVinCi version 1.1.3 for Windows 7**********
**********Multicomparision for the three groups (A, B, C) **********

| Information | Value |
| --- | --- |
| Kruskal-Wallis chi-squared | 97.632414 |
| p-value | 6.30E-22 |
| Degree of freedom | 2 |

**********End Kruskal-Wallis analysis**********

Here the treatment and control groups are shown below:

A: Treatment group (1.0 W/cm2)

B: Treatment group (2.0 W/cm2)

C: Control group (0 W/cm2)

# D. Transducer displacement amplitude

The transducer displacement amplitude was calculate by:

$$A = \sqrt{\frac{2I}{(\rho c)\omega^2}}$$

Where $A$ is the displacement amplitude, the intensity $I$ of the ultrasound is provided by the device manufacturer, ρ is the density of stainless steel (typical material for transducers), c is the longitudinal propagation speed of the ultrasound, and ω is the angular velocity.

$$\omega = 2 \cdot \pi \cdot f$$

$\omega$ is the angular velocity and $f$ is the angular frequecny. The parameters used to calculate ultrasound displacement amplitude are presented in Table D1.

Table D1. Parameters used in calculating ultrasound displacement amplitude.

| Parameter | Value | Reference |
|---|---|---|
| $I$ (W/cm$^2$) | 1 | Ultrasound manufacturer's data (JC-2902) |
| $\rho$ (g/cm$^2$) | 7.8 | (Ghosh 2018) |
| $c$(mm/s) | 5.8 | (Ghosh 2018) |
| $f$(Hz) | 1000000 | Ultrasound manufacturer's data (JC-2902) |

Respective units were converted to calculate equations.

# E. Appendix: Literature review about the ultrasound effects on the extracellular matrix production

| Results | Doses | Cell type | Interpretation | Reference |
|---|---|---|---|---|
| Increase in collagen types I and III, concentration of TGF-b | 1.0 MHz, 20%, 0, 0.1, 0.5, 1.0 W/cm$^2$, 5 min | tendon cells (collagen-coated dish) | Ultrasound stimulates the expression of type I and type III collagen in a process that is likely mediated by the upregulation of TGF-b. ELISA assay (p=0.043). | (Tsai et al. 2006) |
| Increase in cell numbers and collagen deposition | 1.0 MHz, 20%, 0.2 W/cm$^2$, 5 min, every 24 h for 10 days. | HDF cells Fibroblasts encapsulated in calcium | pulsed low-intensity ultrasound alone shows a positive effect on cell proliferation and collagen deposition even without growth factor supplements | (Bohari et al. 2015) |
| 50-67% increase in the rate of collagen synthesis | 1.0 MHz, 20%, 100%, 0.4 W/cm$^2$, 3 min, every 24 h for 9 days. | Tendon fibroblasts – | Ultrasound stimulates collagen synthesis in tendon fibroblasts in | (Ramirez et al. 1997a) |

| | | | | |
|---|---|---|---|---|
| | | Matrix digestion with collagenase (injury model) | response to an injury of the connective tissue matrix and that ultrasound stimulates cell division during periods of rapid cell proliferation. | |
| Increases in collagen of 48%, 57%, and 52% (1.0 MHz) and ranging from 37% to 44% (45 kHz) | 1.0 MHz (20%), 01, 0.4, 0.7 W/cm$^2$; 45 kHz (100%), 15, 50 mW/cm$^2$, 5 min. | Gingival fibroblast | Therapeutic ultrasound induces in vitro cell proliferation and collagen production. | (Doan et al. 1999) |
| Down-regulate the expression of fibronectin and collagen type I.<br>Increase in cell growth. | 3 MHz, 100%, 125, 250, 500, 1000 mW/cm$^2$, 5 min. | Periodontal ligament cells (PDL) | Ultrasound influences the production of key extracellular matrix antigens in vitro and, thus, the functional activities of these cells. | (Harle et al. 2001b) |
| Cells maintained their shape and cell integrity.<br>Decrease in cell growth values after 48 h | 1.0 MHz, 10%, 20%, 0, 0.2, 0.6 W/cm$^2$, 2 min, every 24 h for 4 days. | L929 fibroblast cells (Mouse conjunctive tissue) | Low and medium intensities decreased cell damage, which establishes that acoustic pulsed energy induces the | (Franco de Oliveira et al. 2011) |

| | | | | |
|---|---|---|---|---|
| | | | proliferation of fibroblast cells. | |
| Increase in keratinocyte growth factor (KGF) expression, extracellular regulated kinase (ERK) and c-Jun N-terminal kinase (JNK) activation. Increase in the ERK/JNK ratio. Large vacuoles in the cytoplasm. Decrease in the DNA synthesis 2h after treatment. | 40 kHz, %, 0.002 W/cm$^2$, longest time during which the ultrasound mist did not dislodge cells from the plate surface, measurements 2h, 1,2,3,4 days after treatment | Normal dermal fibroblasts. (Cell scrape-wounded model) | We conclude that ultrasound induces cellular responses that may be beneficial to wound healing. DNA synthesis decreased possibly related to limited cell detachment from the plate. | (Lai and Pittelkow 2007) |
| Increase in the expression of integrins, fibronectin, and paxillin, and activation of focal adhesions via phosphorylation of FAK. | 1.0 MHz, 100%, 100 mW/cm$^2$, 10 min every 24 h for 6 days. | Mesenchymal stem cells (MSCs) from bone marrow (BM) | LIUS stimulation could activate the cell adhesion process and increase the colony-forming ability of MSCs during the early stage of primary culture, without | (Choi et al. 2011) |

| | | | | |
|---|---|---|---|---|
| | | | affecting their phenotypes and multi-potency. LIUS could be a useful tool to obtain a large amount of MSCs for various therapeutic applications | |
| Decrease in cell growth Lower Nuclear Division Index Clastogenic damage (DNA breakage) by the increases of CREST-negative micronuclei frequencies confirmed also by H2AX phosphorylation | 1.0 MHz, 10%, 20%, 0.3, 0.5 W/cm$^2$, 2 min every 24 h for 3 days. | Primary human fibroblasts (AG01522) and MCF-7 human breast adenocarcinoma | US exposure is able to damage the genome integrity. DNA breakage is explained by the fact that cavitation produces reactive oxygen species (ROS). Increase of CREST-positive micronuclei frequencies was due to the damage exerted on microtubules of the mitotic spindle, which is known to cause a mitotic delay. | (Udroiu et al. 2018) |
| Increase cell viability | 1.0 MHz, 200, 300 mW/cm$^2$, 5, 10, 15, 30 min. | L929 lineage | Ultrasound became a resource with promising results in scar healing; that is | (Oliveira et al. 2015) |

| | | | | |
|---|---|---|---|---|
| | | | related to the fact that increased release of growth factors, increased permeability, membrane, intracellular calcium diffusion, and transportation of substances by no-thermal effects. | |
| Different pattern of fibroblast migration and altered cell morphology. | 35 kHz | Fibroblasts | Migration was more varied and widely distributed across multiple angles. The potential implications of these findings on collagen placement in the extracellular matrix, which may affect degree of soft tissue scarring, should be further investigated. | (Conner-Kerr et al. 2015) |
| Ultrasound treatment stimulates tenocytes proliferation and | 1.0 MHz, 20%, 50%, 100%, 0.3, 0.1 W/cm$^2$, 20 min. | Rat tenocytes | Significantly enhanced matrix metallopro- teinase 13 (MMP-13), c-Fos, and c-Jun gene expression, | (Chao et al. 2011) |

| | | | | |
|---|---|---|---|---|
| regulates their matrix metabolism through the cross-talk between TGF-β and ultrasound-induced mitogen-activated protein kinases (MAPKs) signaling pathways | | | increased JNK and p38, but not extracellular signal-regulated kinase-1/2 (ERK1/2), phosphorylation at 5 min, and sustained up to 60 min. SB431542 (transforming growth factor-beta (TGF-β) receptor kinases inhibitor) suppressed ultrasound-induced MMP-13 and c-Fos gene expression, and p38 phosphorylation | |

# References

Abercrombie M. The cells. J Clin Pathol 1978;12:1–6.

Alberts B, Johnson A, Lewis J. The self-assembly and dynamic structure of cytoskeletal filaments. Mol Biol Cell 4th editio. New York: Garland Science, 2002. Available from: https://www.ncbi.nlm.nih.gov/books/NBK26862/

Algaer E. Thermal conductivity of polymer materials. Eidesstattliche Erklärungen, 2010.

Allsop G, Peckham M. Cytoskeleton and Cell Motility. Compr Biotechnol Elsevier, 2011. pp. 191–204. Available from: http://linkinghub.elsevier.com/retrieve/pii/B9780080885049004499

Ananthakrishnan R, Guck J, Wottawah F, Schinkinger S, Lincoln B, Romeyke M, Moon T, Ka J. Quantifying the contribution of actin networks to the elastic strength of fibroblasts. J Theor Biol 2006;242:502–516.

Atherton P, Lausecker F, Harrison A, Ballestrem C. Low-intensity pulsed ultrasound promotes cell motility through vinculin-controlled Rac1 GTPase activity. J Cell Sci 2017;130:2277–2291. Available from: http://jcs.biologists.org/lookup/doi/10.1242/jcs.192781

Baker KG, Robertson VJ, Duck F a. A review of therapeutic ultrasound: biophysical effects. Phys Ther. 2001. pp. 1351–8. Available from: http://www.ncbi.nlm.nih.gov/pubmed/11444998

Bandyopadhyay S, Quinn TJ, Scandiuzzi L, Basu I, Partanen A, Tomé WA, Macian F, Guha C. Low-Intensity Focused Ultrasound Induces Reversal of Tumor-Induced T Cell Tolerance and Prevents Immune Escape. J Immunol 2016;196:1964–1976. Available from: http://www.jimmunol.org/lookup/doi/10.4049/jimmunol.1500541

Bise R, Kanade T, Yin Z, Huh S. Automatic cell tracking applied to analysis of cell migration in wound healing assay. Conf Proc . Annu Int Conf IEEE Eng Med Biol Soc

IEEE Eng Med Biol Soc Annu Conf 2011;2011:6174–9. Available from: http://www.ncbi.nlm.nih.gov/pubmed/22255749

Bjordal JM, Johnson MI, Lopes-Martins RAB, Bogen B, Chow R, Ljunggren AE. Short-term efficacy of physical interventions in osteoarthritic knee pain. A systematic review and meta-analysis of randomised placebo-controlled trials. BMC Musculoskelet Disord 2007 [cited 2016 Apr 12];8:51. Available from: http://www.pubmedcentral.nih.gov/articlerender.fcgi?artid=1931596&tool=pmcentrez&rendertype=abstract

Bohari M. Effect of ultrasound on production of extracellular matrix by cells in culture. The University of Birmingham, 2011.

Bohari SP, Grover LM, Hukins DW. Pulsed low-intensity ultrasound increases proliferation and extracelluar matrix production by human dermal fibroblasts in three-dimensional culture. J Tissue Eng 2015;6:2041731415615777. Available from: http://www.ncbi.nlm.nih.gov/pubmed/26668710%5Cnhttp://www.pubmedcentral.nih.gov/articlerender.fcgi?artid=PMC4674020

Cambier D, D'Herde K, Witvrouw E, Beck M, Soenens S, Vanderstraeten G. Therapeutic ultrasound: temperature increase at different depths by different modes in a human cadaver. J Rehabil Med 2001;33:212–215. Available from: http://www.ncbi.nlm.nih.gov/pubmed/11585152

Cárdenas-Sandoval R, Romero-Malagón D, Grazón-Alvarado D. Effect of Therapeutic Ultrasound on Fibroblast Proliferation In Vitro. In: Braidot A, Hadad A, eds. VI Lat Am Congr Biomed Eng CLAIB 2014, Paraná, Argentina 29, 30 31 Cham: Springer International, 2014. pp. 215–217. Available from: http://dx.doi.org/10.1007/978-3-319-13117-7_56

Cárdenas Sandoval RP, Garzón-Alvarado DA, Ramírez Martínez AM. A mathematical model of the process of ligament repair: effect of cold therapy and mechanical stress. J Theor Biol 2012 [cited 2013 Nov 27];302:53–61. Available from: http://www.ncbi.nlm.nih.gov/pubmed/22381538

Carmine Pappalettere IM, Tachibana K. Effect of Different Ultrasound Frequency Sweep Pattern on Leukemic Cells. Proc World Congr Electr Eng Comput Syst Sci (EECSS 2015) Barcelona, 2015. pp. 1–2.

Carrer V de M, Setti JAP, Veronez D da L, Moser AD. Continuous therapeutic ultrasound in the healing process in rat skin. Fisioter em Mov 2015;28:751–758. Available from: http://www.scielo.br/scielo.php?script=sci_arttext&pid=S0103-51502015000400751&lng=en&tlng=en

Chao YH, Tsuang YH, Sun JS, Cheng CK, Chen MH. The cross-talk between transforming growth factor-beta1 and ultrasound stimulation during mechanotransduction of rat tenocytes. Connect Tissue Res 2011;52:313–321.

Charly Daniel D. Effects of ultrasound therapy with taping PNF training and PNF training with taping in treatment and rehabilitation of sports injuries of high ankle sprain. J Dr NTR Univ Heal Sci 2017;6:92. Available from: http://www.jdrntruhs.org/text.asp?2017/6/2/92/208003

Chen J. Nanobiomechanics of living cells: a review. Interface Focus 2014;4:20130055–20130055. Available from: http://rsfs.royalsocietypublishing.org/cgi/doi/10.1098/rsfs.2013.0055

Chen T, Wu C, Tang M, Huang J, Su F. Complexity of the Tensegrity Structure for Dynamic Energy and Force Distribution of Cytoskeleton during Cell Spreading. PLoS One 2010;5:1–11.

Choi WH, Choi BH, Min B-H, Park. SR. Low-intensity ultrasound increased colony forming unit-fibroblasts of mesenchymal stem cells during primary culture. Tissue Eng Part C 2011;17:517–526.

Codan B, Martinelli V, Mestroni L, Sbaizero O. Atomic force microscopy of 3T3 and SW-13 cell lines: an investigation of cell elasticity changes due to fixation. Mater Sci Eng 2013;33:3303–8. Available from: http://www.ncbi.nlm.nih.gov/pubmed/23706214

COMSOL Multiphysics 5.3. Focused ultrasound induced heating in tissue phantom. 2018. Available from: https://www.comsol.com/model/focused-ultrasound-induced-heating-in-tissue-phantom-12659

Conner-Kerr T, Malpass G, Steele A, Howlett A. Effects of 35 kHz, Low-frequency Ultrasound Application In Vitro on Human Fibroblast Morphology and Migration Patterns. OSTOMY WOUND Manag 2015;61:34–41. Available from: http://search.ebscohost.com/login.aspx?direct=true&db=edswsc&AN=000370316000003&site=eds-live

Cottrell JA, Turner JC, Arinzeh TL, O'Connor JP. The Biology of Bone and Ligament Healing. Foot Ankle Clin 2016;21:739–761.

Dale KM, Bailey JR, Moorman CT. Surgical Management and Treatment of the Anterior Cruciate Ligament/Posterolateral Corner Injured Knee. Clin Sport Med Elsevier Inc, 2017;36:105–117. Available from: http://myaccess.library.utoronto.ca/login?url=http://search.ebscohost.com/login.aspx?direct=true&db=rzh&AN=120577259&site=ehost-live

De Deyne PG, Kirsch-Volders M. In vitro effects of therapeutic ultrasound on the nucleus of human fibroblasts. Phys Ther 1995;75:629–34. Available from: http://www.ncbi.nlm.nih.gov/pubmed/7604082

Díaz BP, Fernández TJM. Ultrasonidos : actualización en patología musculoesquelética. Rehabil 2002;36:303–308.

Dinno M, Dyson M, Young S, Mortime A, Hart J, Crum L. The significance of membrane changes in the safe and effective use of therapeutic and diagnostic ultrasound. Phys Med Biol 1989;34:1543–152.

Doan N, Reher P, Meghji S, Harris M. In vitro effects of therapeutic ultrasound on cell proliferation, protein synthesis, and cytokine production by human fibroblasts, osteoblasts, and monocytes. J Oral Maxillofac Surg 1999;57:409–19; discussion 420. Available from: http://www.ncbi.nlm.nih.gov/pubmed/10199493

Draper DO, Prentice WE. Therapeutic Ultrasound. In: Prentice WE, Quillen WS, Underwood F, eds. Ther Modalities Rehabil 4e New York, NY: The McGraw-Hill Companies, 2011. Available from: http://mhmedical.com/content.aspx?aid=8138750

Dutton M. Anatomy and Biomechanics of the Musculoskeletal System. In: Dutton M, ed. Dutton's Orthop Surviv Guid Manag Common Cond New York, NY: McGraw-Hill, 2011. Available from: http://accessphysiotherapy.mhmedical.com/content.aspx?bookid=467&sectionid=40079842

Dyson M. Non-thermal cellular effects of ultrasound. Br J Cancer Suppl 1982 [cited 2016 May 23];5:165–71. Available from: http://www.pubmedcentral.nih.gov/articlerender.fcgi?artid=2149297&tool=pmcentrez&rendertype=abstract

Eggers J, Onks C. Modalities. In: Mitra R, ed. Princ Rehabil Med New York, NY: McGraw-Hill Education, 2019. Available from: http://accessmedicine.mhmedical.com/content.aspx?aid=1159835072

Farcic TS, Baldan CS, Cattapan CG, Parizotto NA, João SMA, Casarotto RA. Treatment time of ultrasound therapy interferes with the organization of collagen fibers in rat tendons. Brazilian J Phys Ther 2013 [cited 2016 May 23];17:263–71. Available from: http://www.ncbi.nlm.nih.gov/pubmed/23966143

FDA. Summary of safety and effectiveness: Konix sterile gel. 2014.

Foote M. Connective tissue. Salem Press Encyclopedia of Science., 2017.

Franco de Oliveira R, Pires Oliveira DAA, Pacheco Soares C. Effect of low-intensity pulsed ultrasound on l929 fibroblasts. Arch Med Sci 2011;7:224–229.

Franze K. The mechanical control of nervous system development. Development Oxford University Press for The Company of Biologists Limited, 2013 [cited 2017 Dec 4];140:3069–77. Available from: http://www.ncbi.nlm.nih.gov/pubmed/23861056

Freitas TP, Gomes M, Fraga DB, Freitas LS, Rezin GT, Santos PM, Silveira PC, Paula MM, Pinho R a, Streck EL. Effect of therapeutic pulsed ultrasound on lipoperoxidation and fibrogenesis in an animal model of wound healing. J Surg Res Elsevier Ltd, 2010 [cited 2013 Aug 23];161:168–71. Available from: http://www.ncbi.nlm.nih.gov/pubmed/19577772

Fu SC, Shum WT, Hung LK, Wong MWN, Ling Qin, Chan KM. Low-intensity pulsed ultrasound on tendon healing: A study of the effect of treatment duration and treatment initiation. Am J Sports Med 2008;36:1742–1749.

Geltmeier A, Rinner B, Bade D, Meditz K, Witt R, Bicker U, Bludszuweit-Philipp C, Maier P. Characterization of dynamic behaviour of MCF7 and MCF10A cells in ultrasonic field using modal and harmonic analyses. PLoS One 2015;10:1–20.

Ghosh A. Calculating displacement amplitude of ultrasonic power transducer. Physics (College. Park. Md). 2018 [cited 2017 Nov 11]. Available from: https://physics.stackexchange.com/questions/53371/calculating-displacement-amplitude-of-ultrasonic-power-transducer

Gonzalo-Garijo MÁ, Pérez-Calderón R, Pérez-Rangel I, Sánchez-Vega S. Gel transmisor de ultrasonidos: una causa infrecuente de urticaria a frigore. Med Clin (Barc) 2011;136:179. Available from: http://linkinghub.elsevier.com/retrieve/pii/S0025775309016327

Goulet F, Germain L, Poole AR, Auger FA. Tendons and ligaments. In: Lanza R, Langer R, Vacanti J, eds. Princ Tissue Eng (Third Ed Academic Press, 2007. pp. 909–918.

Guilak F, Haider MA, Setton LA, Laursen T, Baaijens FPT. Multiphasic models of cell mechanics Farshid. In: Mofrad MRK, Kamm RD, eds. Cytoskelet Mech Model Meas New York: Cambridge University Press, 2006. p. 256.

Guz N, Dokukin M, Kalaparthi V, Sokolov I. If Cell Mechanics Can Be Described by Elastic Modulus: Study of Different Models and Probes Used in Indentation Experiments. Biophys J Biophysical Society, 2014;107:564–575. Available from: http://dx.doi.org/10.1016/j.bpj.2014.06.033

Haase K, Pelling AE, Haase K. Investigating cell mechanics with atomic force microscopy. J R Soc Interface 2015;12:1–16.

Harle J, Salih V, Mayia F, Knowles J, Olsen I. Effects of ultrasound on the growth and function of bone and periodontal ligament cells in vitro. Ultrasound Med Biol 2001a [cited 2013 Aug 23];27:579–586. Available from: http://linkinghub.elsevier.com/retrieve/pii/S0301562900003264

Harle J, Salih V, Mayia F, Knowles J, Olsen IO. Efects of ultrasound on the growth and function of bone and periodontal ligament cells in vitro. Ultrasound Med Biol 2001b;27:579–586.

Harris CM. Absorption of sound in air versus humidity and temperature. J Acoust Soc Am 1966;40:148–159. Available from: http://asa.scitation.org/doi/10.1121/1.1910031

Hauser RA, Dolan EE, Phillips HJ, Newlin AC, Moore RE, Woldin BA. Ligament Injury and Healing : A Review of Current Clinical Diagnostics and Therapeutics. open Rehabil J 2013;6:1–20.

Henshaw DR, Attia E, Bhargava M, Hannafin JA. Canine ACL Fibroblast Integrin Expression and Cell Alignment in Response to Cyclic Tensile Strain in Three-Dimensional. J Orthop Res 2006;24:481–90.

Hill GE, Fenwick S, Matthews BJ, Chivers R a, Southgate J. The effect of low-intensity pulsed ultrasound on repair of epithelial cell monolayers in vitro. Ultrasound Med Biol 2005 [cited 2013 Aug 23];31:1701–6. Available from: http://www.ncbi.nlm.nih.gov/pubmed/16344132

Hingorani R, Deng J, Elia J, McIntyre C, Mittar D. Detection of Apoptosis Using the BD Annexin V FITC Assay on the BD FACSVerse™ System. BD Biosci. 2011.

Hoh JH, Schoenenberger C a. Surface morphology and mechanical properties of MDCK monolayers by atomic force microscopy. J Cell Sci 1994;107:1105–1114. Available from: http://www.ncbi.nlm.nih.gov/pubmed/7929621

Ingber DE. Tensegrity I . Cell structure and hierarchical systems biology. J Cell Sci 2003;116:1157–1173.

Iranmanesh I, Ohlin M, Ramachandraiah H, Ye S, Russom A, Wiklund M. Acoustic micro-vortexing of fluids, particles and cells in disposable microfluidic chips. Biomed Microdevices Biomedical Microdevices, 2016;18:1–7. Available from: http://dx.doi.org/10.1007/s10544-016-0097-4

Izadifar Z, Babyn P, Chapman D. Mechanical and Biological Effects of Ultrasound: A Review of Present Knowledge. Ultrasound Med Biol 2017;43:1085–1104.

Jacobs CR, Huang H, Kwon RY. Introduction to Cell Mechanics and Mechanobiology. 1st ed. New York: Garland Science, 2012.

Jaganathan, Saravana Kumar Subramanian AP, Vellayappan MV, Balaji A, Aruna John A, Jaganathan AK, Supriyanto E. Natural frequency of cancer cells as a starting point in cancer treatment. Curr Sci 2016;110:1828–1832.

Jiang YY, Park JK, Yoon HH, Choi H, Kim CW, Seo YK. Enhancing Proliferation and ECM Expression of Human ACL Fibroblasts by Sonic Vibration. Prep Biochem Biotechnol 2015;45:476–490. Available from: http://www.ncbi.nlm.nih.gov/pubmed/24842289

Jönsson M. Ultrasound Artefacts. Lund University, 2015.

Justus CR, Leffler N, Ruiz-Echevarria M, Yang L V. In vitro Cell Migration and Invasion Assays. J Vis Exp 2014;1–8. Available from: http://www.jove.com/video/51046/in-vitro-cell-migration-and-invasion-assays

Karlsson LK, Junker JPE, Grenegård M, Kratz G. Human Dermal Fibroblasts: A Potential Cell Source for Endothelialization of Vascular Grafts. Ann Vasc Surg 2009;23:663–674.

Knight KL, Draper DO. Therapeutic ultrasound. Ther modalities art Sci 2nd ed. Baltimore: Lippincott Williams & Wilkins, 2013. pp. 252–282.

Kuznetsova TG, Starodubtseva MN, Yegorenkov NI, Chizhik S, Zhdanov RI. Atomic force

microscopy probing of cell elasticity. Micron 2007 [cited 2014 May 26];38:824–33. Available from: http://www.ncbi.nlm.nih.gov/pubmed/17709250

Lai J, Pittelkow MR. Physiological effects of ultrasound mist on fibroblasts. Int J Dermatol 2007;46:587–93. Available from: http://www.ncbi.nlm.nih.gov/pubmed/17550557

Larson J. Ligaments. Salem Press Encyclopedia of Science, 2017.

Leng X, Shang J, Gao D, Wu J. Low-intensity pulsed ultrasound promotes proliferation and migration of HaCaT keratinocytes through the PI3K / AKT and JNK pathways. Brazilian J Med Biol Res 2018;51:1–8.

Lennart DJ. Nonthermal effects of therapeutic ultrasound: the frequency resonance hypothesis. J Athl Train 2002;37:293–9. Available from: http://www.pubmedcentral.nih.gov/articlerender.fcgi?artid=164359&tool=pmcentrez&rendertype=abstract

Lepeschkin WW, Goldman DE. Effects of ultrasound on cell structure. J Cell Physiol 1952;40:383–397.

Leung MCP, Ng GYF, Yip KK. Therapeutic ultrasound enhances medial collateral ligament repair in rats. Ultrasound Med Biol 2006 [cited 2013 Aug 23];32:449–52. Available from: http://www.ncbi.nlm.nih.gov/pubmed/16530104

Liang C-C, Park AY, Guan J-L. In vitro scratch assay: a convenient and inexpensive method for analysis of cell migration in vitro. Nat Protoc 2007;2:329–333. Available from: http://www.nature.com/doifinder/10.1038/nprot.2007.30

Lochab J, Singh VR. Acoustic behaviour of plastics for medical applications. Indian J Pure Appl Phys 2004;42:595–599.

Louw TM, Budhiraja G, Viljoen HJ, Subramanian A. Mechanotransduction of Ultrasound is Frequency Dependent Below the Cavitation Threshold. Ultrasound Med Biol 2013 [cited 2017 Apr 11];39:1303–1319. Available from: https://www.ncbi.nlm.nih.gov/pmc/articles/PMC4183372/pdf/nihms443566.pdf

Lu H, Qin L, Fok P, Cheung W, Lee K, Guo X, Wong W, Leung K. Low-intensity pulsed ultrasound accelerates bone-tendon junction healing: A partial patellectomy model in rabbits. Am J Sports Med 2006;34:1287–1296.

Lucia U. Bioengineering thermodynamics of biological cells. Theor Biol Med Model Theoretical Biology and Medical Modelling, 2015;12:29. Available from: http://www.tbiomed.com/content/12/1/29

Mahaffy R, Park S, Gerde E, Kas J, Shih C. Quantitative Analysis of the Viscoelastic Properties of Thin Regions of Fibroblasts Using Atomic Force Microscopy. Biophys J 2004;86:1777–1793. Available from: http://linkinghub.elsevier.com/retrieve/pii/S0006349504742459

Man J, Shelton RM, Cooper PR, Landini G, Scheven B a. Low intensity ultrasound stimulates osteoblast migration at different frequencies. J Bone Miner Metab 2012 [cited 2013 Dec 14];30:602–7. Available from: http://www.ncbi.nlm.nih.gov/pubmed/22752127

Managuli V, Roy S. Asymptotical Correction to Bottom Substrate Effect Arising in AFM Indentation of Thin Samples and Adherent Cells Using Conical Tips. Exp Mech Experimental Mechanics, 2018;1–9.

Mcgarry JG, Prendergast PJ. A three-dimensional finite element model of an adherent eukaryotic cell. Eur Cells Mater 2004;7:27–34.

Menikou G, Damianou C. Acoustic and thermal characterization of agar based phantoms used for evaluating focused ultrasound exposures. J Ther Ultrasound Journal of Therapeutic Ultrasound, 2017;5:1–14.

Michalczyk K, Ziman M. Nestin structure and predicted function in cellular cytoskeletal organisation. Histol Histopathol 2005;20:665–671.

Miller D, Smith N, Bailey M, Czarnota G, Hynynen K, Makin I. Overview of therapeutic ultrasound applications and safety considerations. J Ultrasound Med 2012;31:623–634.

Mizera A, Gambin B. Modelling of ultrasound therapeutic heating and numerical study of the dynamics of the induced heat shock response. Commun Nonlinear Sci Numer Simul Elsevier, 2011 [cited 2019 Feb 22];16:2342–2349. Available from: https://www.sciencedirect.com/science/article/pii/S1007570410002686

Mohammed T, Murphy MF, Lilley F, Burton DR, Bezombes F. The effects of acoustic vibration on fibroblast cell migration. Mater Sci Eng C Elsevier B.V., 2016;69:1256–1262. Available from: http://dx.doi.org/10.1016/j.msec.2016.07.037

Morishita K, Karasuno H, Yokoi Y, Morozumi K, Ogihara H, Ito T, Hanaoka M, Fujiwara T, Fujimoto T, Abe K. Effects of Therapeutic Ultrasound on Range of Motion and Stretch Pain. J Phys Ther Sci 2014;26:711–715.

National Center for Biotechnology Information. Compound Summary for CID 2762693. 2019.

Ng CO., Ng GY., See EK., Leung MC. Therapeutic ultrasound improves strength of achilles tendon repair in rats. Ultrasound Med Biol 2003 [cited 2013 Dec 30];29:1501–1506. Available from: http://linkinghub.elsevier.com/retrieve/pii/S0301562903010184

Nick P. Mechanics of the Cytoskeleton. In: P W, ed. Mech Integr Plant Cells Plants Signal Commun Plants vol 9. Springer, Berlin, Heidelberg, 2011. pp. 53–90.

Nijenhuis N, Zhao X, Carisey A, Ballestrem C, Derby B. Combining AFM and acoustic probes to reveal changes in the elastic stiffness tensor of living cells. Biophys J Biophysical Society, 2014;107:1502–1512. Available from: http://dx.doi.org/10.1016/j.bpj.2014.07.073

Nikolaev NI, Müller T, Williams DJ, Liu Y. Changes in the stiffness of human mesenchymal stem cells with the progress of cell death as measured by atomic force microscopy. Biomech Elsevier, 2014;47:625–630. Available from: http://dx.doi.org/10.1016/j.jbiomech.2013.12.004

Noriega S, Hasanova G, Subramanian A. The effect of ultrasound stimulation on the cytoskeletal organization of chondrocytes seeded in 3D matrices. Cells Tissues Organs 2013;197:14–26.

O'Brien Jr. WD. Ultrasound-biophysics mechanisms. Prog Biophys Mol Biol 2007 [cited 2015 Sep 10];93:212–255. Available from: http://linkinghub.elsevier.com/retrieve/pii/S0079610706000915

Ofek G, Wiltz DC, Athanasiou KA. Contribution of the Cytoskeleton to the Compressive Properties and Recovery Behavior of Single Cells. Biophys J Biophysical Society, 2009;97:1873–1882. Available from: http://dx.doi.org/10.1016/j.bpj.2009.07.050

Oliveira PD De, Oliveira DAAP, Martinago CC, Célia R, Frederico P, Soares CP, Oliveira RF De. Effect of low-intensity pulsed ultrasound therapy on a fibroblasts cell culture. Fisioter e Pesqui 2015;22:112–118.

Onishi K, Higuchi M, Asakura T, Masuyama N, Gotoh Y. The PI3K-Akt pathway promotes microtubule stabilization in migrating fibroblasts. Genes to Cells 2007;12:535–546.

Özdemir O. Current cancer treatment : novel beyond conventional approaches / monograph. InTech, 2011 [cited 2019 Feb 22]. Available from: https://www.researchgate.net/publication/328686983_Mathematical_Modelling_of_Breast_Cancer_Thermo-therapy_Treatment_Ultrasound-based_Approach

Palmer JS, Boyce MC. Constitutive modeling of the stress–strain behavior of F-actin filament networks. Acta Biomater Elsevier, 2008 [cited 2018 Aug 2];4:597–612. Available from: https://www.sciencedirect.com/science/article/pii/S1742706108000056

Park BK, Woo Y, Jeong D, Park J, Choi TY, Simmons DP, Ha J, Kim D. Thermal conductivity of biological cells at cellular level and correlation with disease state. J Appl Phys 2016;119. Available from: http://dx.doi.org/10.1063/1.4953679

Pasternak MM, Strohm EM, Berndl ESL, Kolios MC. Properties of cells through life and death - an acoustic microscopy investigation. Cell Cycle 2015;14:2891–2898.

Pedraza Mejías C, Martínez Cañadas J. Respuesta fisiológica del tejido conjuntivo de músculos y tendones tras la aplicación de los agentes físicos. Fisioterapia Elsevier, 2008 [cited 2018 May 20];30:279–285. Available from: http://linkinghub.elsevier.com/retrieve/pii/S0211563808000217

Pollard TD, Borisy GG. Cellular motility driven by assembly and disassembly of actin filaments. Cell 2003;112:453–465.

Pozzi D, Fattibene P, Viscomi D, Di Giambattista L, Grimaldi P, Udroiu I, Bedini A, Giliberti C, Palomba R, Congiu Castellano A. Use of EPR and FTIR to detect biological effects of ultrasound and microbubbles on a fibroblast cell line. Eur Biophys J 2011 [cited 2013 Oct 7];40:1115–20. Available from: http://www.ncbi.nlm.nih.gov/pubmed/21866359

Ramirez A, Schwane J, McFarland C, Starcher B. The effect of ultrasound on collagen synthesis and fibroblast proliferationin vitro. Med Sci Sport Exerc 1997a [cited 2013 Oct 3];29:326–32. Available from: http://ovidsp.tx.ovid.com/sp-3.10.0b/ovidweb.cgi?&S=KMNAFPNCOIDDCLNNNCNKBHMCIDBHAA00&Link+Set=S.sh.22%7C1%7Csl_11226036

Ramirez A, Schwane J, McFarland C, Starcher B. The effect of ultrasound on collagen synthesis and fibroblast proliferationin vitro. Med Sci Sport Exerc 1997b;29:326–332.

Read PJ, Oliver JL, De Ste Croix MBA, Myer GD, Lloyd RS. Neuromuscular Risk Factors for Knee and Ankle Ligament Injuries in Male Youth Soccer Players. Sport Med 2016;46:1059–1066. Available from: http://link.springer.com/10.1007/s40279-016-0479-z

Rincón Cardozo DF, Camacho Casas JA, Rincón Cardozo PA, Sauza Rodríguez N. Abordaje del esguince de tobillo para el médico general. Rev la Univ insdustrial santander 2015;47:85–92.

Robertson VJ, Baker KG. A review of therapeutic ultrasound: effectiveness studies. Phys Ther 2001;81:1339–1350.

Rodríguez M. Ultrasonidos. Electroterapia en Fisioter 2nd ed. Madrid: Panamericana, 2008. pp. 515–544.

Roper JA, Williamson RC, Bally B, Cowell CA, Brooks R, Stephens P, Harrison AJ, Bass MD. Ultrasonic Stimulation of Mouse Skin Reverses the Healing Delays in Diabetes and Aging by Activation of Rac1. J Invest Dermatol Nature Publishing Group, 2015;135:2842–2851.

Roper J, Harrison A, Bass MD. Induction of Adhesion-dependent Signals Using Low-intensity Ultrasound. J Vis Exp 2012;0:1–6.

Samandari M, Abrinia K, Mokhtari-Dizaji M, Tamayol A. Ultrasound induced strain cytoskeleton rearrangement: An experimental and simulation study. J Biomech Elsevier Ltd, 2017;60:39–47. Available from: http://linkinghub.elsevier.com/retrieve/pii/S002192901730297X

Schulze KD, Zehnder SM, Urueña JM, Bhattacharjee T, Sawyer WG, Angelini TE. Elastic modulus and hydraulic permeability of MDCK monolayers. J Biomech Elsevier Ltd, 2017;53:210–213. Available from: http://dx.doi.org/10.1016/j.jbiomech.2017.01.016

Schuster A, Schwab T, Bischof M, Klotz M, Lemor R, Degel C, Schäfer KH. Cell specific ultrasound effects are dose and frequency dependent. Ann Anat 2013;195:57–67.

Shekofteh M, Mohseny M, Shahbodaghi A, Zayeri F, Rahimi F. The Correlation among Y-Index and Other Scientometric Indicators. Curr Sci 2016;110:1823–1828. Available from: http://www.currentscience.ac.in/Volumes/110/9/1828.pdf

Shiran M-B, Shakeri-Zadeh A, Jafarian Dehkordi F, Ghadiri H, Khoei S. Thermal Distribution of Ultrasound Waves in Prostate Tumor: Comparison of Computational Modeling with In Vivo Experiments. ISRN Biomath 2013;2013:1–4.

Shyh-Hau W, Yu-Shuang J, Chien-Hao C, Wen-Tyng L, Jui-Hsiang H. Fibroblast proliferation dependence on insonification of low intensity ultrasounds at different duty cycles. Ultrasonic 2003;1:242–245.

Simon A, Durrieu M-C. Strategies and results of atomic force microscopy in the study of

cellular adhesion. Micron 2006 [cited 2014 May 30];37:1–13. Available from: http://www.ncbi.nlm.nih.gov/pubmed/16171998

Solon J, Levental I, Sengupta K, Georges PC, Janmey PA. Fibroblast adaptation and stiffness matching to soft elastic substrates. Biophys J 2007;93:4453–4461.

Solovchuk MA, Sheu TW, Thiriet M. Image-based computational model for focused ultrasound ablation of liver tumor. J Comput Surg 2014 [cited 2019 Feb 22];1:4. Available from: https://computationalsurgery.springeropen.com/articles/10.1186/2194-3990-1-4

Span LFR, Pennings AHM, Vierwinden G, Boezeman JBM, Raymakers RAP, de Witte T. The dynamic process of apoptosis analyzed by flow cytometry using Annexin-V/propidium iodide and a modified in situ end labeling technique. Cytometry 2002;47:24–31.

Sparrow KJ, Finucane SD, Owen JR, Wayne JS. The effects of low-intensity ultrasound on medial collateral ligament healing in the rabbit model. Am J Sport Med 2005 [cited 2013 Aug 23];33:1048–56. Available from: http://www.ncbi.nlm.nih.gov/pubmed/15888724

Spitalnik P. Histology laboratory manual 2015-2016. 2015.

Springer Nature. Cell migration. © Springer Nature Publishing AG, 2019 [cited 2019 Mar 4]. Available from: https://www.nature.com/subjects/cell-migration

Stricker J, Falzone T, Gardel M. Mechanics of the F-actin Cytoskeleton. J Biomech 2010;43:1–12.

Swaminathan V, Mythreye K, O'Brien ET, Berchuck A, Blobe GC, Superfine R. Mechanical stiffness grades metastatic potential in patient tumor cells and in cancer cell lines. Cancer Res 2011;71:5075–80.

Tarnaud T, Joseph W, Martens L, Tanghe E. Computational Modeling of Ultrasonic Subthalamic Nucleus Stimulation. IEEE Trans Biomed Eng 2018 [cited 2019 Feb

22];1–1. Available from: https://ieeexplore.ieee.org/document/8456629/

Tole NM. Intensity of ultrasound. In: Ostensen H, ed. Basic Phys Ultrason Imaging Malta: World health organization, 2005. pp. 33–34.

Trendowski M, Christen TD, Zoino JN, Acquafondata C, Fondy TP. Generation and Quantitative Analysis of Pulsed Low Frequency Ultrasound to Determine the Sonic Sensitivity of Untreated and Treated Neoplastic Cells. J Vis Exp 2015;1–12. Available from: http://www.jove.com/video/53060/generation-quantitative-analysis-pulsed-low-frequency-ultrasound-to

Trepat X, Chen Z, Jacobson K. Cell Migration. Compr Physiol 2012;2:2369–2392.

Tsai W-C, Chen JY-S, Pang J-HS, Hsu C-C, Lin M-S, Chieh L-W. Therapeutic ultrasound stimulation of tendon cell migration. Connect Tissue Res 2008;49:367–373. Available from: http://www.tandfonline.com/doi/full/10.1080/03008200802325359

Tsai W-C, Pang J-HS, Hsu C-C, Chu N-K, Lin M-S, Hu C-F. Ultrasound Stimulation of Types I and III Collagen Expression of Tendon Cell and Upregulation of Transforming Growth Factor b. J Orthop Res 2006 [cited 2018 Apr 3];24:1310–1316. Available from: https://onlinelibrary.wiley.com/doi/pdf/10.1002/jor.20130

Udroiu I, Marinaccio J, Bedini A, Giliberti C, Palomba R, Sgura A. Genomic damage induced by 1-MHz ultrasound in vitro. Environ Mol Mutagen Wiley-Blackwell, 2018 [cited 2018 Sep 18];59:60–68. Available from: http://doi.wiley.com/10.1002/em.22124

Uhlemann C, Heinig B, Wollina U. Therapeutic ultrasound in lower extremity wound management. Int J Low Extrem Wounds 2003 [cited 2013 Dec 12];2:152–7. Available from: http://www.ncbi.nlm.nih.gov/pubmed/15866839

Unterberger MJ, Schmoller KM, Bausch AR, Holzapfel GA. A new approach to model cross-linked actin networks: Multi-scale continuum formulation and computational analysis. J Mech Behav Biomed Mater Elsevier, 2013 [cited 2018 Aug 2];22:95–114. Available from:

https://www.sciencedirect.com/science/article/pii/S1751616112003311

Van Den Bekerom M, Van Der Windt D, Ter Riet G, Van Der Heijden G, Bouter L. Therapeutic ultrasound for acute ankle sprains ( Review ). Cochrane Database Syst Rev 2011;1–34.

van den Bekerom MPJ, Kerkhoffs GMMJ, McCollum G a, Calder JDF, van Dijk CN. Management of acute lateral ankle ligament injury in the athlete. Knee Surg Sports Traumatol Arthrosc 2013 [cited 2013 Sep 3];21:1390–5. Available from: http://www.ncbi.nlm.nih.gov/pubmed/23108678

Vicente-Manzanares M. Cell migration at a glance. J Cell Sci 2005;118:4917–4919.

Wagner OI, Rammensee S, Korde N, Wen Q, Janmey PA. Softness, strength and self-repair in intermediate filament networks. Exp Cell Res 2009;313:2228–2235.

Warden SJ, Avin KG, Beck EM, DeWolf ME, Hagemeier MA, Martin KM. Low-intensity pulsed ultrasound accelerates and a nonsteroidal anti-inflammatory drug delays knee ligament healing. Am J Sports Med 2006a;34:1094–1102.

Warden SJ, Avin KG, Beck EM, DeWolf ME, Hagemeier MA, Martin KM. Low-intensity pulsed ultrasound accelerates and a nonsteroidal anti-inflammatory drug delays knee ligament healing. Am J Sports Med 2006b [cited 2014 Jan 4];34:1094–102. Available from: http://www.ncbi.nlm.nih.gov/pubmed/16476921

Warden SJ, Metcalf BR, Kiss ZS, Cook JL, Purdam CR, Bennell KL, Crossley KM. Low-intensity pulsed ultrasound for chronic patellar tendinopathy: a randomized, double-blind, placebo-controlled trial. Rheumatology (Oxford) 2008 [cited 2013 Dec 15];47:467–71. Available from: http://www.ncbi.nlm.nih.gov/pubmed/18270224

Wheaton MT, Jensen N. The Ligament Injury-Osteoarthritis Connection: The Role of Prolotherapy in Ligament Repair and the Prevention of Osteoarthritis. J Prolotherapy 2011;3:790–812.

William E. Prentice. Understanding and Managing the Healing Process Through

Rehabilitation. In: Hoogenboom B, Voight M, Prentice W, eds. Musculoskelet Interv Tech Ther Exerc 3rd ed. New York: McGraw-Hill, 2013.

Woo S-Y, Debski RE, Zeminski J, Abramowitch SD, Chan Saw SS, Fenwick JA. Injury And Repair Of Ligaments And Tendons. Annu Rev Biomed Eng 2000;2:83–118.

Wu J, Nyborg WL. Ultrasound, cavitation bubbles and their interaction with cells. Adv Drug Deliv Rev 2008;60:1103–1116.

Yadollahpour A. Ultrasound Therapy for Wound Healing : A Review of Current Techniques and Mechanisms of Action. J Pure Appl Microbio 2014;8:4071–4085.

Ying Z, Lin T, Yan S. Low-intensity pulsed ultrasound therapy: a potential strategy to stimulate tendon-bone junction healing. J Zhejiang Univ Sci B 2012;13:955–963. Available from: http://www.springerlink.com/index/10.1631/jzus.B1200129

Zhang Y. Measuring acoustic attenuation of polymer materials using drop ball test. Aeronautical University, 2013.

Zhou XY, Xu XM, Wu SY, Zhang ZC, Wang F, Yang YL, Li M, Wei XZ. Low-intensity pulsed ultrasound promotes spinal fusion and enhances migration and proliferation of MG63s through sonic hedgehog signaling pathway. Bone Elsevier Inc., 2018;110:47–57. Available from: https://doi.org/10.1016/j.bone.2018.01.025